Amphibole Geochemistry of the Yanacocha Volcanics, Peru: Evidence for Diverse Sources of Magmatic Volatiles Related to Gold Ores

ISABELLE CHAMBEFORT[1*], JOHN H. DILLES[1], ANTHONY A. LONGO[1, 2]

October 29, 2012

[1] DEPARTMENT OF GEOSCIENCES, WILKINSON HALL 104, OREGON STATE UNIVERSITY, CORVALLIS OR 97331-5506, U.S.A.

[2] DEPARTMENT OF GEOSCIENCES, UNIVERSITY OF NEVADA, LAS VEGAS, 4505 S. MARYLAND PKWY, LAS VEGAS, NV 89154-4010, U.S.A.

[*]Corresponding Author:
ISABELLE CHAMBEFORT
GNS Science - Te Pu Ao
Wairakei Research Centre
114 Karetoto Rd, Wairakei, Taupo, 3377
New Zealand
phone: +64 7376 0130
Fax: +64 7374 8199
email: i.chambefort@gns.cri.nz

ABSTRACT

The Yanacocha mining district is located in the Andes of northern Peru in an area of relatively thick continental crust (~35 km) and long-lived Cenozoic subduction-related volcanism. Volcanic activity in the district began at ~20 Ma, and gold deposits (total resource of ~1500 tonnes of gold) are spatially and temporally associated with eruption of the ~80 km^3 Miocene Yanacocha Volcanics from 14.5 to 8.4 Ma. The Yanacocha Volcanics consist of five successive eruptive groups: the Atazaico Andesite lavas, the Colorado Pyroclastics (andesite-dacite), the Azufre Andesite (and dacite) lavas, the San Jose Ignimbrite and related domes (dacite), and small volumes of Coriwachay Dacite dikes, domes and rhyolite ignimbrite. Most dacite magmas likely did not erupt, but rather are inferred to have episodically crystallized to granite at depth to produce ore fluids.

Two distinct populations of amphiboles, distinguished by their aluminum content, are found in the dacites. On the basis of phase equilibrium, the low-aluminum (low-Al) amphiboles were formed at 750–840°C and 110–240 MPa, whereas the high aluminum (high-Al) amphiboles are estimated to have formed at 900-950°C and P_{H2O} > 250 MPa. The trace element contents of amphibole and whole-rocks are consistent with crystallisation of the high-Al amphibole at near-liquidus temperatures from a basaltic-andesite to andesite magma, whereas the low-Al amphibole crystallized at lower temperatures in equilibrium with a rhyolitic melt derived from a crystal-rich dacite magma.

Hydrogen isotopic compositions of both high- and low-Al amphibole exhibit a large range from -40‰ to -120‰ for the 12.5 to 11.0 Ma andesite-dacite and have a restricted range from -100‰ to -112‰ for the younger Coriwachay Dacite (10.8 to 8.4 Ma). The high δD values of some high-Al amphiboles (-41‰) likely represent subduction-derived water dissolved in a water- and fluorine-rich, chlorine-poor, and sulfate-saturated basaltic andesite magma. This magma was injected into an upper crustal, chlorine-rich, silicic magma chamber characterized by low δD of low-Al amphibole (-60‰ or lower). Short residence times (<1 yr) of high-Al amphibole in the upper crustal chamber are estimated from dehydration rims and hydrogen diffusion lengths. Following the eruption of the lower San Jose Ignimbrite at 11.5 Ma, a new shallow dacite magma chamber was established and minor amounts of mafic magma input continued, as shown by the high-Al amphiboles present in the San Jose domes and in the middle and upper San Jose Ignimbrite. These high-Al amphiboles (δD_{Amph} = -81‰ to -102‰) had sufficiently long residence time (>1 year) in the shallow chambers prior to eruption to equilibrate isotopically with the predominant low-δD dacite. The young Coriwachay Dacite magmas likely assimilated meteoric-hydrothermally altered low-δD rocks to generate the low δD of the low-Al amphibole (-100‰ to -120‰). These dacites are related to the main gold ore stages, and contain low-Al amphibole that is zinc- and chlorine-rich, but copper- and fluorine-poor, compared to the associated high-Al amphibole.

These results imply that deep mafic magmas may have supplied much of sulfur, fluorine, copper, and by inference gold, whereas upper crustal recycling may have supplied a significant proportion of the water and chlorine to the late dacite magmas and ore fluids.

Keywords: amphibole; assimilation; hydrogen isotopes; mixing; volatiles; gold ores.

INTRODUCTION

Magmatic volatiles play a major role in the evolution of arc magmas and are essential for the ormation of magmatic-hydrothermal ore deposits (Burnham, 1979; Carroll & Holloway, 1994). Water is the dominant volatile in such magmas, but is commonly accompanied by sulfur, chlorine, carbon dioxide, and in certain cases fluorine, dependent on the magma composition and oxygen fugacity (Wallace, 2005). Magmatic cooling, crystallization, and ascent commonly result in exsolution of magmatic volatiles that may form magmatic-hydrothermal ore deposits such as porphyry copper (Mo-Au) and high-sulfidation (Au-Cu) epithermal deposits (Hedenquist & Lowenstern, 1995). Water, chlorine and sulfur species are directly responsible for most of the complexation and transport of ore metals and other species both within a single high pressure supercritical fluid phase or at low pressure as binary mixtures of vapor and brine (Candela & Piccoli, 1995; Pokrovski *et al.*, 2008).

This study focuses on understanding the origin of magmatic volatiles in the Yanacocha Volcanics, which erupted over the period from 14.5 to 8.4 Ma and are contemporaneous with, genetically related to, and host one of the largest known clusters of epithermal high-sulfidation deposits globally with an aggregate resource of >50 million ounces (>1500 t) of gold (Longo *et al.*, 2010; Teal & Benavides, 2010). The rocks in this volcanic series commonly contain amphibole and other volatile-bearing mineral phases that can be used to decipher the magmatic volatile contents and conditions during emplacement, cooling, crystallization, and eruption (e.g., Burnham, 1979; Oberti *et al.*, 1993; Sato *et al.*, 1997). Furthermore, the composition of the amphibole and coexisting plagioclase can be used to estimate temperature-pressure conditions in the magmas (e.g., Blundy & Holland, 1990; Anderson & Smith, 1995). Amphibole breakdown to produce reaction rims of various widths can be used to estimate magma degassing rates under changing pressure-temperature conditions (Rutherford & Hill, 1993; Rutherford & Devine, 2003). A companion paper by Longo *et al.* (2010) documents the Ar-Ar geochronology, volcanology, and petrology-geochemistry of the Yanacocha Volcanics, and their relation to gold mineralization in the district.

YANACOCHA VOLCANICS

The gold deposits of the Yanacocha district are located approximately 18 km north of Cajamarca city, northern Peru, and are hosted by the Yanacocha Volcanics (Longo *et al.*,

2010). Volcanic activity began with eruption of "pre-Yanacocha Volcanics," the Calipuy Group volcanic rocks, that include the Tual and Chaupiloma or lower andesite lahars from 20 to 16 Ma, and the younger and dacitic Cerro Fraile pyroclastic unit at 15.5 Ma (Fig. 1). Longo *et al.* (2010) define the Yanacocha Volcanics as constituting *ca.* 88 km^3 of magma erupted from 14.5 to 8.4 Ma in an area 20 km by 30 km centered on the Yanacocha mining district and including five periods of magmatic activity and five eruptive groups (Figs. 1 and 2) based on ^{40}Ar-^{39}Ar ages and bulk-rock compositions (cf., Chiaradia *et al.*, 2009; Teal & Benavides, 2010). Volcanism began with the lava eruptions of the Atazaico Andesite (14.5-13.3 Ma), followed by eruptions of andesite and dacite ignimbrites of the Colorado Pyroclastics that were accompanied by minor intrusions and lavas (12.6-12.1 Ma). The Colorado Pyroclastics were closely followed by eruptions of silicic andesite to dacite lavas of the Azufre Andesite (12.1-11.7 Ma). The San Jose Ignimbrite overlies the Azufre Andesite and includes three andesite to dacite ignimbrite members (lower, middle, upper; 11.5, 11.2, and 11.2 Ma, respectively) that are associated with three San Jose dacite dome complexes, erupted atop the eruptive vents of the ignimbrites (11.4, 11.3, and 11.2 Ma; Figs. 1 and 2). The youngest rock unit is the Coriwachay Dacite that includes biotite-bearing porphyritic dikes and domes (10.8, 9.9, 8.4 Ma), as well as the rhyolitic Negritos ignimbrite (8.4 Ma). The main hydrothermal events associated with the ore deposition postdate the San Jose Ignimbrite and range from ~ 11 to 8 Ma (Longo *et al.*, 2010). The

Yanacocha igneous rocks are typically phenocryst-rich and range from 25-55 vol.% total phenocrysts in lavas, 30-60 vol.% phenocrysts in domes, and 40 to 70 vol.% in the fines-depleted ignimbrites (Fig. 2; Longo *et al.*, 2010). They have geochemical compositions typical of a subduction-related, medium-K, calc-alkaline suite that temporally evolved from early basaltic andesite and andesite to late dacite and rhyolite (Longo, 2005; Chiaradia *et al.*, 2009; Longo *et al.*, 2010; Supplementary Data Table DR1).

In addition to plagioclase and amphibole, all units of the Yanacocha Volcanics have accessory Fe-Ti oxides, apatite, zircon and in some cases pyroxene, biotite, alkali feldspar or titanite as illustrated by the characteristic modal mineralogy shown in Figure 2. The details of the mineralogy are given in the Supplementary Data. Anhydrite is a common but sparse inclusion in amphibole and pyroxene (Chambefort *et al.*, 2008).

PETROGRAPHY OF AMPHIBOLE: LOW- AND HIGH-AL POPULATIONS

Amphibole is the dominant ferromagnesian mineral in most Yanacocha igneous rocks and forms euhedral to subhedral phenocrysts (Fig. 3; Chambefort *et al.*, 2008; Longo *et al.*, 2010). Amphibole phenocryst abundance, size, and shape, are variable throughout the volcanic stratigraphy (Figs. 2-4). Amphiboles in the pre-Yanacocha Tual and Chaupiloma andesite and the dacitic Cerro Fraile pyroclastic deposits represent 5 to 10 modal percent; the phenocrysts vary in length from 0.7 to 3.5 mm (Longo, 2005). In the Yanacocha

Volcanics, amphibole phenocrysts are generally larger (up to 5 mm long) in the intrusions than in the lavas and pyroclastic rocks, although amphibole megacrysts (up to 1 cm) are found in the lower San Jose Ignimbrite (Sample RC-6).

High-Al amphibole is the only amphibole present in the Atazaico and Azufre Andesites, where it forms small prismatic to subhedral crystals (0.2 to 2.5 mm long) that may contain inclusions of Fe-Ti oxides, cloudy-textured apatite, and rarely pyroxene or plagioclase or anhydrite (Figs. 3 and 4). Petrographically and chemically distinct high-Al and low-Al amphibole are both present in the Colorado Pyroclastics, San Jose Ignimbrite, and San Jose domes, and in these rocks high-Al amphibole forms subhedral to euhedral grains that range from 1 to 10 mm long and commonly contains small inclusions of apatite, anhydrite and in some cases Fe-Ti oxides, but only rarely contain inclusions of plagioclase and pyroxene (Figs. 3 and 4). Low-Al amphibole crystals commonly are subhedral, <3 mm long, and contain sparse inclusions of Fe-Ti oxides, plagioclase, and pyroxene, and micro-inclusions of apatite and anhydrite (only in San Jose Ignimbrite). In the Coriwachay dacite porphyries, the low-Al amphiboles are up to 1 cm long, subhedral to euhedral, and commonly contain 50 vol.% inclusions of biotite, plagioclase, and Fe-Ti oxides (Figs. 3h and 4h). Anhydrite is present as sparse inclusions in amphibole and pyroxene in all units of the Yanacocha Volcanics, except the last-erupted rhyolitic Negritos ignimbrite, and generally has a subhedral “crystalline” form but has an unusual “wormy” texture where it is

extremely abundant and accompanied by high-sulfur apatite in high-Al amphibole in the Lower San Jose Ignimbrite (Fig. 4c,d; Chambefort et al., 2008).

Most amphibole phenocrysts in the Yanacocha Volcanics are subhedral in shape or have breakdown coronas or interior zones (Figs. 3 and 4), suggesting reaction with melt prior to solidification of the host magma. Nonetheless, because high-Al and low-Al amphiboles are both present in the same rocks they must have formed under different pressure-temperature or melt composition conditions, and therefore cannot be in equilibrium with one another. The two amphibole populations are found together as a result of magma mixing of relatively brief duration either in a subvolcanic magma chamber or in the eruption conduit of pyroclastic flows.

Some large, anhydrite-rich high-Al amphiboles from sample RC-6 are euhedral, unzoned, and show no evidence of breakdown (Figs. 3d and 4c,d; Chambefort *et al.*, 2008). In contrast, some high and low-Al amphiboles show distinct reaction textures. Three main types of amphibole reaction textures are apparent. The simplest is a resorbtion texture characterized by a subhedral or, rarely, anhedral amphibole outline but no new minerals replacing the amphibole rim (Fig. 3e). This resorbtion texture is most readily apparent in back-scattered electron images where concentric compositional growth bands are truncated at the amphibole-melt interface (Fig. 4g) but is also suggested by the anhedral edges of grains (Fig. 4f). The edge of the amphibole is commonly smooth and gently curved on faces

such as {110} parallel to the c-axis, but may be irregular on the {011} terminations as a result of amphibole dissolution on {110} cleavages (Fig. 4f). Weakly to strongly developed dissolution textures are common on high-Al amphiboles in the Atazaico and Azufre Andesite lavas, as well as in all members of the San Jose Ignimbrite and the San Jose domes. In the middle San Jose Ignimbrite, low-Al amphibole sometimes displays irregular embayments filled with groundmass glass in sample VC-1 (Fig. 3e). The observed resorbtion textures are consistent with either heating or chemical disequilibrium with the melt. These textures are not consistent with growth in the presence of two or more immiscible fluids or with growth of skeletal or negative crystal shapes characteristic of undercooling and rapid crystal growth or lack of supply of chemical components to the growing crystal (e.g. Sobolev & Kostyuk, 1975; Roedder, 1984; Lowenstern, 1995).

A second amphibole reaction texture is a corona or breakdown rim that most commonly consists of fine-grained plagioclase, pyroxene, and Fe-Ti oxides (Fig. 3c), but in some cases consists of only plagioclase and Fe-Ti oxides (Fig. 3b,f). These coronas are developed on both high-Al and low-Al amphibole. Although there are some wide coronas (>200 μm) that are accompanied by partial breakdown of the interior of both high-Al and low-Al amphibole (Figs. 3c & 4a), the most common rims are narrow and developed on amphibole cores that are stable. High-Al amphiboles in the Azufre Andesite lavas are characterized by coronas (Fig. 3c, Fig. 4b) that are narrow or absent on prismatic amphibole

faces ({110}, {010}) but 20-40 μm wide on c-axis crystal terminations {011}. Low-Al amphiboles in the Colorado Pyroclastics display wider coronas 25-60 μm in width on {110} faces (Fig. 3b). In the San Jose Ignimbrite and domes, breakdown coronas are relatively rare on both high-Al and low-Al amphiboles. Amphibole breakdown coronas such as these have been described to be the result of either ascent, depressurization, and water-loss, or via heating above the temperature conditions of amphibole stability (Rutherford & Hill, 1993; Rutherford & Devine, 2003). The associated sieve-textured plagioclase (Longo, 2005) has been interpreted in other studies as resulting from heating associated with high-temperature magma injection and mixing (Coombs *et al.*, 2000).

The third type of amphibole decomposition observed includes "opacite" or Fe-Ti oxide rims (Fig. 3a) that when narrow are commonly difficult to distinguish from plagioclase-rich breakdown coronas. Where opacite rims are wide the amphibole has been converted to red-brown oxy-hornblende via a process that is generally attributed to hydrogen-loss or oxidation during ascent and depressurization (Rutherford & Hill, 1993; Demény *et al.*, 2006). Back-scattered electron images demonstrate that opacite is commonly hematite replacing the rims and {110} cleavages of amphibole (Fig. 4a), and that the opacite was produced after any amphibole resorbtion and as a separate event from corona breakdown. Opacite is common in many high-Al amphiboles of the Atazaico and Azufre Andesite lavas, the upper San Jose Ignimbrite, and San Jose domes.

ANALYTICAL TECHNIQUES

Amphibole phenocrysts were analyzed for major elements, both *in-situ* in thin sections of rocks and in separated grains mounted in epoxy plugs, using a Cameca SX100 electron microprobe at Oregon State University, a 30 nA current, 15 kV accelerating potential and 2 μm beam diameter. Laser-ablation ICP-MS analyses of trace elements in amphibole were performed in the W.M. Keck Collaboratory for Plasma Mass Spectrometry at Oregon State University using a VG ExCell quadrupole ICP-MS and NewWave DUV 193 nm ArF Excimer laser system, with He as the sweep gas. General analytical conditions were similar to those in Kent *et al.* (2004) and employed laser spots 70 μm in diameter and pulse rates of ~5 Hz during 115 seconds. ^{43}Ca was used as the internal isotopic standard, and analyses were quantified with reference to multiple replicate analyses of NIST 612 and NIST 610 standard glasses under similar ablation conditions. Comparison of analyses of NIST 612 and NIST 610 suggests accuracy better than 10% (2σ stdev) for all elements reported.

Single grains of whole amphibole for hydrogen isotopic analysis were attached unpolished atop a 2.54 cm glass slide and analyzed by electron microprobe semi-quantitatively to identify low-Al and high-Al amphiboles. This method was effective to identify the amphibole type whenever the total oxide exceeded 90 wt %. Amphibole grains selected in this manner from 26 samples were analyzed (n = 76) for their hydrogen isotopic composition using a High Temperature Conversion Elemental Analyzer coupled with a

continuous flow isotope ratio mass spectrometer (TCEA-IRMS) at the Oregon State University, using a He carrier gas at 0.5 bar pressure. Aliquots of 1.5 to 3 milligrams of amphibole were rapidly heated at 1430°C in the TCEA furnace to liberate structurally bound water, which was reacted with glassy carbon to produce H_2 and CO gases. The H_2 gas was separated using a gas chromatograph column operating at 100°C (Sharp *et al.*, 2001), its deuterium/hydrogen (D/H) ratio was analyzed in a Finnigan Mat Delta XL mass spectrometer. NBS-30 biotite and OSU Butte BUD96014 biotite were analyzed repeatedly every fifth analysis as an internal mineral standard in each run of TCEA analyses to assess the tank H_2 reference gas. All data are reported in per mil (‰) relative to V-SMOW. Replication of NBS-30 yielded $\delta D = -64.3 \pm 1.7‰$ (2σ stdev; n=42), and of Butte biotite yielded $\delta D = -158.4 \pm 3.4‰$ (n=35). Accuracy is considered to be ± 2‰ (2σ stdev).

Additionally, six high-Al and two low-Al amphibole samples were mounted in indium metal, and analyzed for hydrogen isotopes (n=16) and volatile abundances (n=29) using the 6f Cameca secondary ion mass spectrometer (SIMS) at the Carnegie Institution of Washington following techniques described by Hauri *et al.* (2002). The hydrogen isotope data obtained by SIMS have been corrected for mass fractionation associated with matrix effects using an empirical procedure based on each amphibole's composition following Hauri *et al.* (2002). Accuracy is considered better than ± 5 ‰ (2σ stdev), with replication for the Kipawa amphibole $\delta D = -84 \pm 8‰$ (2σ stdev; n=16) relative to V-SMOW. Using the

SIMS, the concentrations of water, CO_2, S, F, and Cl are routinely analyzed with detection limits < 30 ppm for H_2O, < 3 ppm for CO_2, and < 1 ppm for F, S and Cl (Hauri *et al.*, 2002).

AMPHIBOLE COMPOSITIONS

Yanacocha igneous rocks all contain magnesium-rich (Mg>Fe) calcic amphibole that include aluminum-rich and aluminum-poor (high-Al and low-Al) varieties ranging from alkali-rich hastingsite ($Na+K_A>0.5$; $^{VI}Al<Fe^{3+}$) to alkali-poor ($Na+K_A<0.5$) tschermakite (Si<6.5) and hornblende (Si>6.5) calculated on the basis of 23 oxygen equivalents per formula unit (Leake *et al.*, 1997; Table 1 and Supplementary Data Table DR2; Fig. 5). Amphiboles in the pre-Yanacocha units are tschermakite in Tual-Chaupiloma andesites and magnesiohornblende in Cerro Fraile pyroclastic rocks with $(Na+K)_A$ that ranges from 0.1 to 0.4 and 0.1 to 0.3 and Mg-number (molar $Mg/Mg+Fe_{tot}$) that varies from 0.60 to 0.68 and 0.52 to 0.61, respectively. Amphiboles in both units have moderate-Al contents (~10 wt % Al_2O_3) (Table 1; Fig. 5). Amphiboles from lavas in both the Atazaico and Azufre Andesites are aluminum-rich (up to 14 wt % Al_2O_3) magnesiohastingsite with Mg-numbers that range from 0.64 to 0.83 for the Atazaico, and from 0.66 to 0.81 for the Azufre (Fig. 5b; Table 1). Chromium contents in the Atazaico and Azufre high-Al amphibole are the highest of all volcanic rocks at Yanacocha (respectively, Cr_2O_3 < 0.02 to 0.6 wt % and <0.02 to 0.2 wt %; Table 1).

In contrast, two compositional groups of amphibole have been defined based on aluminum content for the Colorado Pyroclastics, the San Jose Ignimbrite, the San Jose domes, and the Corimayo dacite intrusion of the Coriwachay Dacite (Fig. 5). The amphibole compositions are similar in both the Colorado and the San Jose Ignimbrites. High-Al amphiboles (11-13 wt % Al_2O_3) are mainly magnesiohastingsite, with $(Na+K)_A$ from 0.48 to 0.72 for the San Jose Ignimbrite and from 0.38 to 0.63 for the Colorado Pyroclastics (Fig. 5a). Low-Al amphiboles (5-9 wt % Al_2O_3) are principally magnesiohornblende and rare tchermakite, with $(Na+K)_A$ from 0.14 to 0.31 (Fig. 5a; Table 1). Mg-numbers of both high- and low-Al amphibole vary between 0.6 and 0.75 (Fig. 5b). Chromium contents are generally higher for high-Al amphibole compared to low-Al amphibole with up to 0.2 versus <0.05 wt % for *the* Colorado Pyroclastics, and up to 0.11 versus <0.05 wt % for San Jose Ignimbrite, respectively (Table 1). In both the Colorado Pyroclastics and the middle San Jose Ignimbrite a few high-Al amphiboles have overgrowths of low-Al rims (Figs. 2 and 4e). Low-Al magnesiohornblende is the most abundant amphibole in the late Coriwachay Dacite and is characterized by $(Na+K)_A$ ~ 0.3-0.5, Mg-numbers ~ 0.6-0.7, and Cr_2O_3 contents less than 0.05 wt %. Also present are rare high-Al amphibole crystals that lack a reaction rim (Fig. 3h) and have a Mg-numbers of about 0.72 and $(Na+K)_A$ of about 0.57 (Fig. 5). High-Al amphibole commonly displays faint concentric growth zonation in

BSE images (Fig. 4g) that is consistent with modest variation in Mg/(Mg+Fe) (Fig. 5b), but low-Al amphibole displays no apparent zonation.

All high-Al amphiboles in the Yanacocha Volcanics have similar and narrow ranges of rare earth element (REE) contents, consistent with crystallization from similar magmas, and have chondrite-normalized REE patterns that are convex upward with maxima of 10 to 20 times chondrite at Nd (Fig. 6; Table DR2). The high-Al amphiboles generally lack a negative Eu anomaly. In contrast both medium-Al amphiboles of the pre-Yanacocha volcanic rocks (i.e., Tual-Chaupiloma andesites) and the low-Al amphiboles of the Yanacocha Volcanics have distinctive negative Eu anomalies. All the low-Al amphiboles have similar REE patterns and abundances that are commonly 2 to 5 times greater than high-Al amphiboles in units where both amphiboles are present (Fig. 6). Sample RC3 from the middle San Jose Ignimbrite contains zoned high-Al amphibole including one unusual high-Al rim that has a REE composition and Eu anomaly similar to low-Al amphibole in the same sample (Fig. 6d).

Trace element compositions of high-Al and low-Al amphiboles differ significantly on primitive mantle-normalized diagrams, as illustrated by sample DN77 of a Yanacocha porphyry intrusion, which is contemporaneous with the Colorado Pyroclastics (Fig. 7). High-Al amphiboles have trace element patterns and contents similar to both the whole-rock and many other hydrous arc magmas. For example, both high-Al amphibole and the whole-

rock have negative high field strength element (Nb) anomalies and negative anomalies in heavy REE and Y consistent with the presence of garnet in the deep residual mineralogy (Defant & Drummond, 1990), positive anomalies in fluid-mobile elements Ba, Sr and Pb (whole-rock only) and high Sr/Y ratios typical of water-rich magmas in which crystallization of plagioclase is suppressed. Fractionation of high-Al hornblende would be expected to reduce the middle REE contents of residual melts and has been proposed for similar magmas (cf., Rohrlach & Loucks, 2005; Richards, 2011); however, middle REE are not definitively reduced in the Yanacocha Dacites. These trace element anomalies are characteristic of many arc magmas associated with porphyry copper-gold mineralization globally (e.g., Kay & Mpodozis, 2001; figure 15 of Longo *et al.*, 2010).

The low-Al amphiboles have similar, but elevated, trace element contents compared to the high-Al amphiboles and have negative anomalies in Sr, Eu, Ba, V and Ti. The latter anomalies are consistent with the crystallization of the low-Al amphibole from an evolved magma via prior-crystallization of Sr-, Eu-, and Ba-enriched plagioclase and K-feldspar, and Ti- and V-enriched magnetite, titanite, and biotite (Figs. 6 and 7). This is in agreement with petrographic, geochemical and experimental data (Rutherford & Devine, 2008) that the low-Al amphiboles crystallized from shallow, low temperature, hydrous, and oxidized magmas.

Volatile contents of both high-Al and low-Al amphiboles were analyzed by electron microprobe (F, Cl; Table 1), and an additional twenty-five high-Al and two low-Al amphiboles were analyzed by SIMS (H_2O, CO_2, F, Cl, and S, Table 2). Although they vary significantly, high-Al and low-Al amphiboles are generally distinct and characterized by high F/Cl and low F/Cl, respectively (Fig. 8). High-Al amphiboles are Cl-poor in 90% of the analyses (<0.05 wt % Cl) and have a maximum of 0.1 wt % Cl in the upper San Jose Ignimbrite (Fig. 8a). High-Al amphiboles range from F-rich to F-poor (1.3 to <0.1 wt % F, Fig. 8b). The low-Al amphiboles in all the units are F-poor (<0.4 wt % F) and are commonly Cl-rich (>0.05 wt % Cl) compared to high-Al amphibole. The highest Cl contents occur in the upper San Jose Ignimbrite (up to 0.3 wt % at 10 wt % Al_2O_3), and both Cl and Al contents are low in the late Coriwachay Dacites (~0.1 wt % Cl at 6-9 wt % Al_2O_3; Fig. 8a). The high Cl content of the low-Al amphibole in the rapidly erupted San Jose Ignimbrite likely records a magmatic composition, whereas the low Cl content of the Coriwachay dacites may reflect water and Cl loss during slow magma ascent, as noted for other porphyry copper plutonic amphiboles and biotites (Kesler *et al.*, 1975; Dilles, 1987).

The H_2O contents of high-Al amphibole crystals vary considerably, but non-systematically, from 1.17 to 2.04 wt % as determined by SIMS (Fig. 8c, Table 2). High-Al amphiboles from the lower San Jose Ignimbrite (sample RC6) and low-Al amphiboles from the Coriwachay Dacite (sample COR-1) have the highest H_2O contents (Table 2), whereas

high-Al amphiboles from the upper San Jose Ignimbrite (samples BS-3 and CB-38) have the lowest H_2O content (1.17 to 1.43 wt %).

High-Al and low-Al amphiboles analyzed by LA-ICP-MS (Fig. 9; Supplementary Data Table DR2) differ significantly in their Zn and Cu contents in different rock units. Zn contents are typical of igneous amphiboles, range from 60 to 400 ppm and are highest in low-Al amphiboles. As observed in most igneous amphiboles, Zn generally is well correlated with Cl (Fig. 9a), Fe and Mn contents but not with Cu contents (cf., Rowe et al., 2008). Cu contents are generally low (<70 ppm); the low-Al amphiboles from the Coriwachay Dacite associated with the main Au (Cu) mineralization have the lowest Cu (<10 ppm; Fig. 9b). The high-Al amphiboles from the Yanacocha porphyry temporally related to the Colorado Pyroclastics but not closely associated with the Au (Cu) ores, have highest Cu (130-210 ppm, Fig. 9b; Supplementary Data Table DR2). In this sample Cu and Li are positively correlated, similar to amphiboles erupted in 2004-06 from Mount St. Helens where Rowe et al. (2008) proposed that Li and Cu diffused into amphibole from a vapor phase. Note, that in two other Yanacocha amphibole samples, the Li content varies widely from <5 to 150 ppm but Cu is uniformly low (<20 ppm) so there is no systematic behavior of Li and Cu.

HYDROGEN ISOTOPE COMPOSITION OF THE AMPHIBOLE

TCEA hydrogen isotopic analyses

We first examine hydrogen isotope compositions measured by TCEA. Amphibole separates have a large range in δD values from -41 to -120‰ and in water contents (Table 3, Fig. 10); the few biotites (n=3) analyzed range from -102 to -108‰ similar to amphibole in similar-age samples (Table 3). TCEA analyses of high-Al amphibole range from -41 to -111‰, whereas analyses of low-Al amphibole have a slightly lower isotopic range from -66 to -116‰. As a function of age of eruption, the hydrogen isotopic compositions vary widely and are heterogeneous in pre-Yanacocha ~15.5 Ma volcanic units (-62 to -103‰) and in the 12.5 to 11.2 Ma eruptive units of the Yanacocha Volcanics (-41 to -111‰), whereas the three samples from 10.8 to 8.4 Ma of the Coriwachay Dacite contain amphibole and biotite with homogeneous and low δD values with a range from -103 to -116‰ (n=11, Figure 10, Table 3). The Coriwachay dacites are temporally associated with the majority of the hydrothermal gold introduction between ~11 and 8 Ma (Longo *et al.*, 2010; Fig. 10a). No significant variation in the amphibole isotopic compositions occurs between pyroclastic units and temporally associated domes or dykes (Table 3).

Amphiboles with a breakdown rim of Fe-oxide and plagioclase or an opacite rim also display a substantial range of hydrogen isotopic compositions (Table 3). For example, in the units of the San Jose ignimbrite, or the Azufre andesite, the hydrogen isotopic composition determined *via* TCEA ranges from -47 to -95‰ for amphibole without

breakdown rims, to -80 to -107‰ for amphiboles with breakdown rims (Table 3, Figure 10b). The amphiboles with breakdown rims have mean values 15‰ lower that those without rims, e.g., -93.2 ± 9.2‰ (n=20, 1s) compared to -78.5 ± 14.3‰ (n=21).

Discrepancy between TCEA and SIMS hydrogen isotopic analyses

SIMS hydrogen isotopic data for amphiboles range from -19 to -191‰ and are therefore more variable and generally depleted in deuterium relative to the TCEA data. Because the TCEA data are derived from larger samples, were replicated, and are well standardized they are considered to be robust. We focus this discussion on the SIMS data (Fig. 11), which are collected from a very small volume and rely on a standardization that is sensitive to mineral composition (cf., Harford & Sparks, 2001; Hauri *et al.,* 2002). Amphibole breakdown as a result of decreased water pressure produces diffusion of water or hydrogen out of the amphibole to first produce water-poor amphibole, and then with further diffusive loss generates a vacancy in the hydroxyl site that leads to structural instability and breakdown rims of plagioclase-pyroxene-Fe-oxides or opacite (e.g., Harford & Sparks, 2001; Demény *et al.*, 2006). As a result of the H_2O loss a positive correlation between the isotopic composition and the H_2O content is expected, which is weakly observed for the High-Al amphibole at Yanacocha (Fig. 11a; $R^2 = 0.36$). The correlation noted above is partly explained by amphibole dehydration via the reaction $2OH^-_{amph} = O^{2-}$

$_{amph} + H_2O$ as a result of loss of D-enriched water from both the magma and the amphibole (Demény *et al.*, 2006). The Cl and F content and F/Cl ratio of the high-Al amphibole do not vary significantly with the H_2O_{SIMS} content, which suggests that dehydration does not significantly affect the halogen content of amphibole (Table 2, Fig. 8c). Our petrographic observations support such a dehydration process because most of the high-Al amphiboles analysed by SIMS that have low water contents (BS3, CHQS2, CB38; Fig 11a) also have plagioclase-pyroxene-Fe-oxide reaction rims (Figs. 3 and 4). The dehydration process ($2OH^-_{amph} = O^{2-}_{amph} + H_2O$) will not change the oxidation state (Fe^{3+}/Fe_{tot}) of the amphibole, but in contrast the dehydrogenation process ($2OH^-_{amph} + 2e^- = 2O^{2-}_{amph} + H_2$) will increase the oxidation state and Fe^{3+}/Fe_{tot} of the amphibole (Demény *et al.*, 2006). The latter reaction is favored by the higher diffusivity of H_2 compared to H_2O. Yanacocha high-Al amphiboles as a group do not show any correlation of Fe^{3+}/Fe_{tot} ratio with water content (Fig. 11b). Nonetheless, for several analyses of amphiboles from a single sample the Fe^{3+}/Fe_{tot} proportion decreases slightly from ~0.65 to 0.45 as H_2O content decreases by 5 to 10% (Fig. 11b) but there is no clear correlation of water content with δD_{SIMS} (Fig. 11a). Therefore, these amphiboles have an apparent reduction trend accompanying dehydration opposite to the oxidation predicted by the dehydrogenation reaction above. A possible explanation is that dehydration is accompanied by amphibole reduction and O_2 loss via a reaction such as $2OH^-_{amph} = 0.5O^{2-}_{amph} + H_2O + 0.25\ O_2 + e^-$.

Partial amphibole dehydration has been modeled by Demény *et al.* (2006) and produces positive correlations of δD values with water content of amphibole consistent with a water-amphibole fractionation factor of 80‰. Rayleigh distillation models shown by the arrowed paths in Figure 11a suggest 50% loss of the water from amphibole would lower δD values by 60‰, whereas 50% loss of hydrogen would increase δD values by up to 60‰. The maximum water loss for Yanacocha amphiboles is 40%, corresponding to a maximum lowering of 45‰. Therefore, degassing and amphibole dehydration cannot explain amphibole, and by inference magma, δD_{SIMS} isotopic values that vary by more than 100‰ (Figs. 10 and 11a). Taylor (1991) demonstrated that the maximum isotopic fractionation produced by Rayleigh distillation of magma is about 50‰ depletion after 90% of the water has degassed. We conclude that a decrease of δD values by up to 20 to 40‰ may result from degassing during the eruption of each volcanic unit. This is observed in the Azufre Andesite samples where the CHQS2 high-Al amphiboles have a breakdown corona and a composition of ~70‰, whereas sample DO60 amphiboles with no rims have a δD of -40‰.

Our data show major discrepancies, outside of analytical error, between values determined by TCEA and SIMS for ~45% of the samples analyzed by both techniques (Table 3). One explanation could be related to the scale of the analyses. Indeed, SIMS analyses report the *in-situ* composition for a 50 μm diameter by 1-2 deep μm spot (~100 μm^3), whereas in most cases each TCEA analysis was obtained from a single whole crystal

about 100 μm long (~10^6 μm^3). Therefore, it is possible that the SIMS analyses represent isotopic variation inside microdomains, perhaps affected by micrometer-scale degassing in the amphibole phenocrysts, whereas the TCEA analyses represent the bulk isotopic composition, including biotite inclusions in the Coriwachay Dacite (Fig. 4h). Large isotopic variations at the 100 μm scale have been observed by Harford & Sparks (2001), who interpreted that the larger δD_{SIMS} values in the cores compared to rims of amphiboles from Montserrat document assimilation of hydrothermal amphibole whose preserved isotopic composition requires a short residence of weeks within the magma. This explanation could be applied to Yanacocha, but does not explain the apparent depleted isotopic bias of the SIMS analyses. The low δD_{SIMS} values in the range -120 to -191‰ therefore are analytically suspect, or potentially are analyses of hydrothermally altered microfractures. Below, we focus our discussion of magmatic processes on the TCEA analyses.

DISCUSSION

Magmatic Source and Evolution

By analogy with many petrologic studies in the Andes, we propose that the andesites and dacites at Yanacocha were generated by lower- to middle-crustal processes, followed by evolution in transient upper crustal magma chambers (cf., Hildreth & Moorbath, 1988). The Yanacocha magma system evolved from 14.5 to 8.4 Ma, and over the last 4 Myr

involved injections of deep-sourced andesitic melts into a series of upper crustal dacitic magma bodies (Longo *et al.,* 2010). It is likely that most of the dacites did not erupt, and assuming a 5:1 intrusive to extrusive ratio we have estimated that about 400 km^3 of granite episodically crystallized at depth and evolved hydrothermal fluids responsible for the Au (Cu) ores (Chambefort *et al.,* 2008). All these andesites and dacites appear to be characteristic of arc magmas with high water and sulfur contents on the basis of the similar trace element contents of both whole-rocks and amphibole, together with the presence of anhydrite (Longo *et al.,* 2008; Chambefort *et al.,* 2008). Whole-rocks and high-Al amphibole do not have a negative europium anomaly in chondrite-normalized REE patterns (Fig. 6), consistent with the interpretation that the high-Al amphibole crystallized from a mafic melt at high-temperature, near-liquidus conditions in the lower or middle crust. Plagioclase was absent or scarce due to both high temperatures and water pressures. Figure 6 illustrates the whole-rock REE contents compared with calculated REE patterns of the melt in equilibrium with amphibole using partition coefficients for basaltic andesite, calc-alkaline andesite, dacite and rhyolite (Fig. 6; Nagasawa & Schnetzer, 1971; Fujimaki *et al.*, 1984; Irving & Frey, 1984; Sisson, 1994). For equilibrium between high-Al amphibole and melt the use of basaltic andesite partition coefficients yields melt REE compositions similar to whole-rocks for the range of andesites to dacites including the Colorado Pyroclastics and the Atazaico and Azufre Andesites (Figs. 6c-g), whereas use of an andesite-melt partition

coefficient provides the best match to the observed upper San Jose whole-rock REE compositions (Figs. 6b,c).

Low-Al amphibole in dacite has an enriched REE pattern compared to the high-Al amphibole, which supports a similar origin of both dacite and andesite magmas. The low-Al amphiboles, however, have significant negative Eu anomalies and depletions of Ti, V, Sr, Pb, and Ba. This is consistent with the crystallization of plagioclase, Fe-Ti oxides, and biotite during magmatic evolution prior to amphibole formation. For equilibrium between low-Al amphibole and melt, the use of dacite partition coefficients yields calculated melt REE compositions greater than the observed whole-rock composition (Figs. 6d,g), whereas the use of rhyolite-melt partition coefficients yields melt compositions similar to the whole-rock, (Figs. 6b,c,g). The low-Al amphiboles in dacites therefore likely crystallized from relatively low temperature and shallow rhyolite melts, possibly in a dacitic bulk-magma. The origin of the dacitic upper crustal magmas is not well-constrained, but the whole-rock compositional data of Longo *et al.* (2010) and isotopic data of Chiaradia *et al.* (2009) suggest that the dacitic magmas likely formed via two processes: a) ponding of andesitic magma in the upper crust accompanied by assimilation of silicic crustal material or mixing with crustally-derived silicic melts, and b) by deep- to mid-crustal assimilation-fractional crystallization processes. Regardless, the shallow dacitic magma chambers were cooler and more crystalline than the basaltic-andesite injections and crystallized low-Al amphibole.

Note that the low-Al amphiboles yield calculated melt compositions with uneven REE patterns and relatively poor fits to whole-rock patterns, which likely reflect the poorly known, but large crystal/melt partition coefficients characteristic of silica-rich melts.

Pre-eruptive conditions: temperature - pressure – oxygen fugacity

Petrologic estimates provide evidence for magma evolution along a complex path of decreasing temperature and pressure evolving from deep to shallow conditions. High-Al amphibole crystallized at high temperature and in some cases contains anhydrite and sparse apatite inclusions, but no other mineral inclusions (e.g., sample RC6; Chambefort *et al.*, 2008). High-Al amphibole compositions are consistent with crystallization from high-temperature mafic melts of andesite to basaltic-andesite composition as supported by their high Cr contents (up to 0.8 wt %), elevated Mg-numbers (Fig. 5, Table 1) and low REE contents. This reasoning supports the hypothesis that high-Al amphibole was commonly a liquidus phase formed in equilibrium with silicate melts that had low SiO_2/Al_2O_3 ratios (Moore & Carmichael, 1998; Grove *et al.*, 2003, 2005). Experiments by Grove *et al.* (2005) crystallized similar composition amphibole from water-saturated basaltic melts with as much as 12 wt % H_2O at NNO+2 oxidation conditions and ~ 600 MPa.

Application of several amphibole thermobarometers gives a range of estimates for high-Al amphibole crystallization. Temperatures of 800 to 900°C and pressures of 600 to 900 MPa are estimated on the basis of the TiO_2 -Al_2O_3 thermobarometer (1.5 to 2.4 wt %

TiO_2 and 11.9 to 14.5 wt % Al_2O_3, respectively) for basalts of Ernst & Liu (1998). Higher temperatures of 930 to 1000°C are estimated based on the Al^{IV} per formula unit of 1.9 to 2.3 for high-Al amphibole stability experiments on hydrous basalts (Helz, 1973). Application of the empirical amphibole thermobarometer of Ridolfi *et al.* (2010) yields a range of estimated temperatures between 950 and 1000°C and pressures of 400 to 550 MPa. The experimental liquidus temperature of amphibole is 930-950°C in a hydrous Mt. Hood andesite (Eggler & Burnham, 1973) and Mount St. Helens dacite, but 880-910°C in Soufriere Hills andesite at 150-500 MPa (Fig. 12), and 1000°C in hydrous basaltic andesite lacking plagioclase (Moore & Carmichael, 1998). In summary, the Yanacocha high-Al amphibole likely crystallized at 950-900°C and pressures greater than 250 MPa, most likely at 400 to 600 MPa (13 to 20 km depth).

For low-Al amphiboles, the application of the plagioclase-hornblende geothermometer (Blundy & Holland, 1990) and the hornblende geobarometer (Anderson & Smith, 1995) to plagioclase (~$An_{30–40}$) and coexisting amphibole suggest that these minerals equilibrated in the upper crust between 750 and 840°C and 110–240 MPa (4-8 km depth; Table 4). The amphibole thermobarometer of Ridolfi *et al.* (2010) gives a similar range of temperatures between 820 and 900°C, at pressures between 120 and 200 MPa.

The iron-titanium oxide pairs from seven Yanacocha samples yield a narrow range of temperature estimates from 780 to 820°C and strongly oxidized conditions (NNO+1 to

NNO+2.5) using the geothermometer and oxygen barometer of Anderson and Lindsley (1985; Supplementary Data Table DR3). We use these estimates in preference to those from MELTS-2011, which give estimates about 100°C lower (600-760°C), and commonly subsolidus for our samples, as noted by Ghiorso & Evans (2008). Magnetite-rich spinel and ilmenite-rich rhombohedral oxides are present in all rocks, and coexist with titanite in the Corimayo and other dacites younger than 11 Ma at Yanacocha. As implied by the presence of anhydrite (Chambefort *et al.*, 2008), the paucity of magmatic sulfides (Brennecka, 2006), and the local presence of titanite (Dilles, 1987), the estimated oxygen fugacities are high. They range from NNO+1 for early 13.8 Ma Atazaico Andesite to NNO+2 to NNO+2.5 conditions for the 12.6-12.4 Ma Colorado Pyroclastics, the 11.5-11.2 Ma San Jose Ignimbrites, and the 10.7 Ma Corimayo Dome (Fig. 13; Supplementary DataTable DR3). Note that multiple analyses of both magnetite and ilmenite yield a relatively narrow compositional range for each of the five pyroclastic rocks that contain multiple oxide grains likely sampled from a relatively large volume of magma (see Supplementary DataTable DR3). These data support the hypothesis that the Fe-Ti oxides equilibrated in a shallow magma body at a relatively low temperature compared to amphibole and pyroxene temperatures prior to pyroclastic eruptions.

Magma ascent rates from amphibole breakdown

Three petrographic types of amphibole breakdown were outlined above, and are interpreted as follows: 1) resorbtion due to heating; 2) corona development due to magma ascent; and 3) opacite development associated with low-temperature dehydration. The presence or absence of reaction rims on high-Al and low-Al amphiboles provides estimates for the pressure – temperature variations during magma ascent as pioneered by Rutherford *et al.* (1988). Based on the amphibole compositions and phase equilibria presented above we estimate that basaltic andesite to andesitic magmas ascended through the crust with only a small loss of heat and began to crystallize high-Al amphibole at about 950°C at ~600 MPa pressure (20 km depth). High-Al amphiboles from the Atazaico and Azufre Andesite lavas and the Colorado Pyroclastics are mainly characterized by resorbed rims associated with plagioclase with sieved cores, which are consistent with heating and melting of amphibole and plagioclase as a result injection of new magma and consequent mixing (Coombs *et al.,* 2000). Some high-Al amphiboles in these rocks have narrow (20-60 μm) breakdown coronas of plagioclase + pyroxene ± Fe-Ti oxides. The coronas are consistent with amphibole breakdown via depressurization and water loss during ascent (Fig. 12a). Application of experimental amphibole breakdown rates from Rutherford *et al.* (1988), Rutherford & Hill (1993), and Rutherford & Devine (2003) suggest a period of decompression of 10 to 50 days and slow ascent rates (1 to 6 mm/sec) consistent with low

transit of magmas in the upper crust (Table 5). In a few rare cases, thick coronas (>200 μm) suggest magma ascended more slowly, or possibly that the amphibole was sampled by younger magma injections.

In the andesitic to dacitic magmas sampled by the Colorado Pyroclastics, the San Jose Ignimbrite, and the San Jose domes some high-Al amphiboles lack breakdown corona rims, whereas the accompanying low-Al amphiboles have resorbed edges and local narrow opacite rims. It is proposed that the high-Al amphibole resided in hot andesite that was injected into or ponded near the base of a dacitic magma chamber at ~6 to 8 km depth and did not undergo significant decompressive breakdown. The low-Al amphiboles resident in the dacite at 110 to 240 MPa pressure (4-8 km depth) and 750-840°C, however, did undergo breakdown via melting as a result of heating by the hot underplated andesitic magma as proposed for the Mount St. Helens dacite by Rutherford & Hill (1993), for the Fish Canyon Tuff by Bachmann & Bergantz (2003), and for the Soufrière Hills andesite by Rutherford & Devine (2003). The heat required for destabilization of low-Al amphibole can only be estimated, as it is also dependent on magma composition, temperature, and pressure. We estimate heating by 10° to 100° to achieve temperatures of ~850 to 900°C on the basis of the experimental phase equilibria of the Mount St. Helens dacite and Soufrière Hills andesite (Fig. 12b).

Origin of the water in the Yanacocha magmas

The presence of two populations of amphibole that crystallized from different magma compositions, and at different pressures and temperatures in the same rock sample provides direct evidence for polybaric crystallization and recharge in an upper crustal magma reservoir. The Yanacocha amphiboles contain water from two or more distinctly different sources. The highest δD values (-41 to -51‰) of the high-Al amphibole are from the Azufre Andesite and the lower San Jose Ignimbrite (Fig. 10). These compositions likely reflect deep, subduction-derived water incorporated into a basaltic magma that rose and was modified in the lower- and mid-crust by assimilation – fractional crystallization processes (cf., Chiaradia *et al.,* 2009). Using a hornblende-water fractionation factor of -15‰ at 800°C (Graham *et al.*, 1984), these high δD values (-40 to -51‰) would have been in equilibrium with water having δD of -25 to -36 ‰. This composition is similar to the δD range of -25 to -45‰ observed globally for water in silicic arc magmas (Taylor *et al.*, 1983; Taylor, 1991), and δD of -20 to -40‰ for water from degassing arc volcanoes (Giggenbach, 1992, 1997).

The low-Al amphiboles in shallow dacitic magmas have δD values of -65 to -116‰ that are substantially lower than many of the associated high-Al amphiboles. It is calculated that the low-Al amphiboles with δD of –65 to -116‰ would have been in equilibrium with waters having δD of -50 to -100‰, that are substantially lower than the common range of

magmatic waters (-20 to -45‰; Taylor, 1991; Giggenbach, 1992). As argued above, using a hydrogen isotopic fractionation between melt and water of -20‰ (Dobson *et al.*, 1989; Taylor, 1991), loss of 40% of the magmatic water during degassing could have shifted an initial δD_{magma} of -35‰ to as low as -80‰ (Fig. 11a). Therefore, the δD_{magma} values of less than about -80‰ are not explained. Moreover, δD of amphibole in pyroclastic rocks was not likely affected by degassing, because pyroclastic eruptions are characterized by rapid degassing (~1 day-scale) and during these short times hydrogen has a very short diffusion length scale of 50 μm, so only a very small percentage (<1%) of the hydrogen could degass from amphiboles >1 mm in length (Cole & Ohmoto, 1986; Table 5).

The D-depleted hydrogen in amphiboles in dacitic magmas can be only partly explained by partial amphibole dehydration or dehydrogenation during magmatic degassing. This mechanism could have lowered the δD of amphibole by up to 40‰, as modeled by Demémy et al. (2006). Nonetheless for individual samples the water contents and δD_{TCEA} of amphiboles are not correlated and suggest this process produces a maximum D-depletion of about 20 ‰ (Fig. 14a); as noted above comparison of amphiboles with and without breakdown rims suggests D-depletion of 20 ‰. Water-rich amphiboles in the late Coriwachay dacite dikes (δD of -116 ‰) may also be somewhat D-depleted as a result of minor amounts of hydrothermal alteration.

It is considered that the D-depleted hydrogen in amphiboles, and therefore dacitic magmas, is largely due to assimilation of older and hydrothermally altered Yanacocha Volcanics along the roof and sides of the magma chamber(s). There are no hydrogen isotopic analyses of hydrothermal minerals from Yanacocha, but the nearby and similar high-elevation 14.5 Ma-old Pierina high-sulfidation deposit is characterized by clay and alunite with δD ranging from -81 to -126 ‰ and -39 to -97 ‰, respectively (Fifarek & Rye, 2005). Using these low δD compositions as estimates of hydrothermally altered rocks at Yanacocha, we calculate that the Yanacocha low-Al amphiboles and host dacites could have acquired up to 50 % (likely 20-30 %) of their magmatic water via selective assimilation of hydrothermally altered wall-rock. As illustrated in Figure 14, dacite melts with δD of -75 ‰ can be produced by subequal mixtures of andesite (δD of -40 ‰, 4 wt. % H_2O) and an hydrothermally altered wallrock assimilant (50 % quartz and 50 % alunite plus kaolinite, δD = -95 ‰, 6.7 wt. % H_2O). Dacites could contain a relatively large mass proportion (about 20-30%, Fig. 14b) of hydrothermally altered rock because assimilation of such hot and low melting point rock is energetically possible. Similar mechanisms have been widely documented for the oxygen isotopic depletion of granites and "low-^{18}O rhyolites" (Larson & Taylor, 1986; Larson & Geist, 1995; Feeley & Sharp, 1996; Bindeman *et al.*, 2008). Large ^{18}O-depletions of magmas in several of these cases follow ignimbrite eruption, caldera collapse, attendant hydrothermal alteration, and apparent assimilation of

hydrothermally altered rock during renewed magmatism. At Yanacocha, extensive alunite- and clay-rich hydrothermal alteration predates each of the dacitic eruptions containing low δD amphibole, and alunite- and clay-rich lithic fragments are abundant in both the Colorado Pyroclastics and San Jose Ignimbrite. Longo *et al.* (2010, figs. 15-17) report Ar-Ar ages of hydrothermal alunites from Stage 1 (13.6-12.6 Ma) predating the Colorado Pyroclastics (12.6-12.4 Ma), Stage 2 (~11.5 Ma) predating the San Jose Ignimbrites and domes (11.54-11.22 Ma), Stage 3 (11.0-10.7 Ma) predating the Corimayo, La Quinoa, and Punta Negra domes and intrusions of the Coriwachay Dacite (11.0-10.2 Ma), Stage 4 (10.3-9.9 Ma) predating the Yanacocha Dacite Porphyry (9.90 Ma), and Stage 5 (~9.3-8.2 Ma) predating the Yanacocha late Rhyolite and Negritos Ignimbrite (8.4 Ma) (Fig. 10). There is therefore an excellent correlation of precursor hydrothermal activity with eruption of subsequent low δD dacite that is consistent with assimilation of hydrothermally altered rock to produce the low δD magmas.

Figure 15 presents a general magmatic evolution model including the different origins of water at Yanacocha. Deep-sourced basaltic to andesitic water- and F-rich magmas of the early Atazaico Andesite and the later Azufre Andesite contained high-Al amphibole, and were S-rich and oxidized enough to contain a separate sulfate phase (Chambefort *et al.*, 2008). The lavas erupted before and between the two major ignimbrite sequences and contain only high-Al amphiboles consistent with an origin for the andesitic melts from

deeper hydrous basaltic melts modified in lower to middle crustal magma conduits, but with little magma mixing or assimilation at upper crustal levels (Fig. 15a). These more mafic magmas periodically injected into or underplated a shallow (~4-8 km depth) more differentiated dacitic magma chamber that was crystal-rich and contained low-Al amphibole as well as plagioclase, and was equally oxidized (Fig 15b). The two populations of amphibole are found in the Colorado Pyroclastics, San Jose Ignimbrites, and late Coriwachay Dacites and demonstrate that regular mixing processes at Yanacocha occurred during magmatic evolution over a period of >4 million years as also demonstrated by whole rock geochemical variations (fig. 12 of Longo *et al.*, 2010). The injections of deep-sourced, volatile-rich mafic melts may have triggered eruption as at Pinatubo (cf., Pallister *et al.*, 1992).

High-Al amphiboles in the Colorado Pyroclastics and San Jose Ignimbrite are both D-enriched and D-depleted, suggesting that they exchanged locally with hydrogen from the low-D dacitic magma. The lower San Jose Ignimbrite contains large (5 mm long) high-Al amphiboles that in some cases preserve deep-sourced high δD values (-41 to -51 ‰) and in other cases have low δD values of -62 to -85 ‰ that are partially to fully isotopically exchanged (Figs. 14 and 15). The diffusivity of hydrogen in kaersutite amphibole has been experimentally determined by Ingrin and Blanchard (2000) to be fives times greater along the c-axis compared to the b-axis; the latter agrees with diffusivities for actinolite from

Graham et al. (1984). Assuming hydrogen is governed by c-axis diffusion, 1 mm-long amphibole at 800°C reaches >99 % isotopic exchange equilibrium in 33 days and 50 % in 11 days (Table 5). Therefore, the hydrogen diffusivities suggest some high-Al amphiboles had relatively short residence times in the shallow low δD dacitic chamberof less than 11 days in some cases and about 100 days or more in other cases (Fig. 15b).

A new shallow dacitic magma chamber was reestablished within a period of ~0.2 Myr following eruption of the lower San Jose Ignimbrite, and additional andesitic magma input occurred periodically prior to eruption of the middle and upper San Jose Ignimbrites, based on the presence of high-Al amphibole. In these ignimbrites there was a sufficiently long residence time (about 1 yr or more, Table 5) to allow high-Al amphibole from the mafic magma to exchange deuterium-hydrogen completely with the dominant low δD water reservoir of the shallow, more silicic magma. We infer that this is also the time-scale for heating and resorbtion of the low-Al amphiboles in these same magmas. Note that the hydrogen diffusion estimate of residence times of high-Al amphiboles in dacite magmas is similar to or somewhat greater than the magma ascent times estimated from amphibole breakdown coronas, but that both estimates are within error of one another because of the substantial uncertainties of hydrogen diffusivities, amphibole breakdown rates, and amphibole geometries (Table 5).

Subsequent to the eruptions of the San Jose Ignimbrite, a series of San Jose dacitic domes (11.7-11.2 Ma) erupted through the vent sites of the earlier ignimbrites, which also have high-Al amphibole with low δD values of -85 and -95 ‰ consistent with equilibration with D-depleted dacitic magma via assimilation of altered wall-rocks (Fig. 15c). The water contents and petrography of the amphibole suggest little modification after eruption. Similar magmatic conditions were likely reestablished during periodic eruption of the Coriwachay Dacites (10.7-8.4 Ma) that contain biotite with D-depleted δD_{TCEA} of -103 to -116 ‰. By the end of the magmatic history (8.4 Ma), the input of andesitic magma had decreased, and shallow crustal magma chambers had evolved to rhyolite, as sampled by the Yanacocha Lake dike and Negritos ignimbrite.

CONCLUSION AND IMPLICATIONS FOR MAGMA-RELATED ORE DEPOSITS

At Yanacocha, eruptions of about 88 km^3 of magma spanned a 6 Myr period and were dominated by lower- or middle-crust derived andesite magmas containing high-Al amphibole that evolved during the last 4 Myr to produce dacitic upper crustal magma chambers containing low-Al amphibole. A small proportion of the dacite magma erupted episodically as ignimbrites, but most (>80%) is inferred to have crystallized to granite at depth and passively degassed to produce high-sulfidation gold (copper) ores associated with stages 1 through 5 of quartz-alunite alteration (Chambefort et al., 2008; Longo *et al.*, 2010).

The major and trace element and isotopic data for both deep-sourced andesites and shallow dacites are similar and consistent with a cogenetic magmatic system that evolved largely by the well-established but complex processes of crystal fractionation, magma mixing, and assimilation (Longo *et al.*, 2010; Chiaradia *et al.*, 2009). Amphibole major and trace element compositions reported as part of this study suggest that high-Al amphibole, with or without pyroxene and apatite, was the liquidus phase in the basaltic andesite to andesite melts at about 950°C in the middle crust (13-20 km depth), but that low-Al amphibole crystallized together with plagioclase, Fe-Ti oxides, and biotite from dacitic magmas at about 800°C in the upper crust (4-8 km depth).

Andesites supplied most volatiles to the shallow magmatic hydrothermal system. Isotopic compositions of amphibole provide estimates that hydrous andesites contained about 4 wt % water with $\delta D \approx -40$ ‰, and that andesites evolved to dacites in shallow chambers as D-depleted as $\delta D \approx -55$ to -75 ‰ via assimilation of 20-30% low δD (≈ -95 ‰) hydrothermally altered wall-rock. The high-Al amphiboles in the hydrous andesitic magmas have high F and low Cl (0.15-3 wt % and 0.01-0.08 wt %, respectively), low Zn (50-200 ppm), and inclusions of anhydrite and apatite that are consistent with equilibrium with sulfate-rich (>1000 ppm S) melts (Fig. 8; Chambefort *et al.*, 2008). Low-Al amphiboles from shallow dacitic magmas also contain anhydrite inclusions, but have relatively low F and high Cl (0.02-0.05 and 0.1-0.3 wt %, respectively) and higher Zn (200-450 ppm). On

the basis of the high-Al and low-Al amphiboles the deep-sourced andesitic magmas had high S/Cl ≈ 3-10 and dacites had lower S/Cl ≈ 1. While an increase of chlorine by a factor of 2-3 from andesite to dacite may be possible via crystal fractionation prior to separation of a Cl-rich volatile phase, it seems likely that chlorine is also increased in dacite by assimilation of Cl-bearing hydrothermally altered wall-rock. The low-Al amphiboles in the late, ore-associated, Coriwachay dacite are the most enriched in zinc, and display trends to lower chlorine contents consistent with loss of magmatic water and chlorine. Copper contents are low in most amphiboles, suggesting that it remained in the melt or was transferred to a volatile phase. In the shallow dacitic magma chambers, periods of cooling and crystallization resulted in volatile saturation, anhydrite breakdown and transfer of SO_2 to the volatile phase (Chambefort *et al.*, 2008). We hypothesize that slow degassing of magmatic volatiles (>1 yr) from ore-related dacite domes, porphyry intrusions, and the inferred voluminous granites at depth produced magmatic-hydrothermal fluids enriched in sulfur, chlorine, copper, and by inference gold. In contrast, the pyroclastic eruptions of the Colorado Pyroclastics and San Jose Ignimbrites were triggered by injections of high temperature andesite into the shallow dacite magma chambers on a time scale of about 10 days to 1 yr, based on diffusion rates of hydrogen in high-Al amphibole. Low-Al amphibole resorbtion textures document melting induced by these heating events.

The amphibole compositions and geochemistry demonstrate that deep-sourced and volatile-rich basaltic andesite to andesite melts underpin the long-lived Yanacocha magmatic system, but also evolved to a series of late upper crustal dacitic magma chambers in part by assimilation of hydrothermally altered wall-rock that added low δD water and chlorine to the magmas. Furthermore, several episodic upper crustal dacitic magma chambers formed over a 4 Myr time span and either erupted explosively, triggered by injections of hot andesite, or cooled and crystallized to granite plutons at depth and passively degassed to form magmatic-hydrothermal fluids. Thus, we infer that magmatic evolution and ore-formation involves complex processes of upper crustal recycling of volatiles in addition to deep- or mid-crust arc-type magmatic sources of volatiles and metals (cf., Kay & Mpodozis, 2001; Rohrlach & Loucks, 2005).

ACKNOWLEDGEMENTS

The authors thank Adam Kent and Frank Tepley for assistance with the laser ablation ICP-MS and the microprobe analyses, respectively. We also thank Anita Grunder and the VIPER group at OSU, for discussions. T. Feeley, D. Selles, O. Bachmann, M. Rutherford, T. Vennemann, G. Wörner and an anonymous reviewer are greatly acknowledged for their constructive comments.

FUNDING

Funding was provided by the U.S. National Science Foundation grant EAR-0337798 to Dilles and Streck, Swiss Fonds National Grant PBGE2-115088 to Chambefort, and from Minera Yanacocha.

REFERENCES

Andersen, D. J. & Lindsley, D. H. (1985). New (and final!) models for the Ti-magnetite/ilmenite geothermometer and oxygen barometer. Abstract AGU 1985 Spring Meeting Eos Transactions. *American Geophysical Union* **66**, 416.

Anderson, J. L. & Smith, D. R. (1995). The effects of temperature and fO_2 on the Al-in hornblende barometer. *American Mineralogist* **80**, 549-559.

Bachmann, O. & Bergantz, G. W. (2003). Rejuvenation of the Fish Canyon magma body: A window into the evolution of large-volume silicic magma systems. *Geology* **31**, 789-792.

Bacon, C. R. & Hirschmann, M. M. (1988) Mg/Mn partitioning as a test for equilibrium between coexisting Fe-Ti oxides. *The American Mineralogist* **73**, 57–61.

Bindeman, I. N., Fu Bin Kita, N. T. & Valley, J. W. (2008). Origin and evolution of silicic magmatism at Yellowstone based on ion microprobe analysis of isotopically zoned zircons. *Journal of Petrology* **49**, 163-193.

Blundy, J. D. & Holland, T. J. B. (1990). Calcic Amphibole Equilibria and a New

Amphibole-Plagioclase Geothermometer. *Contributions to Mineralogy and Petrology* **104**, 208-224.

Brennecka, G. (2006). Origin and metal content of magmatic sulfides in Cu-Au mineralizing silicic magmas: Yerington, Nevada and Yanacocha, Peru. *Unpublished MS thesis,* Oregon State University, 49 p., http://hdl.handle.net/1957/2076.

Burnham, C. W. (1979). Magmas and hydrothermal fluids. In: Barnes, H. L. (ed.) *Geochemistry of ore deposits 2nd ed.,* Wiley J. & Sons, New York.

Candela, P. A. & Piccoli, P. M. (1995). Model ore–metal partitioning from melts into vapor and vapor/brine mixtures. In: Thompson, J.F.H. (ed.) *Magmas, Fluids, and Ore* Deposits. *Mineralogical Society of Canada,* Nepean, Ontario, Canada **23**, 101–127.

Carmichael, I. S. E. (1967). The iron-titanium oxides of salic volcanic rocks and their associated ferromagnesian silicates. *Contributions to Mineralogy and Petrology* **14**, 36–64.

Carroll M. R. & Holloway, J. R. (1994). *Volatiles in Magmas. Mineralogical Society of America, Reviews in Mineralogy* **30**. 517p.

Chambefort, I., Dilles, J. H. & Kent, A. J. R. (2008). Anhydrite-bearing andesite and dacite as a source for sulfur in magmatic-hydrothermal mineral deposits. *Geology* **36,** 719-722.

Chiaradia, M., Merino, D. & Spikings, R. (2009). Rapid transition to long-lived deep crustal magmatic maturation and the formation of giant porphyry-related mineralization (Yanacocha, Peru). *Earth and Planetary Science Letters* **288**, 505-515.

Cole, D. R. & Ohmoto, H. (1986). Kinetics of isotopic exchange at elevated temperatures and pressures. In: Valley, J. W., Taylor, H. P. & O'Neil, J., R. (eds.) *Stable isotopes in high temperature geological processes. Mineralogical Society, Reviews in Mineralogy* **16**, 41-90.

Coombs, M.L., Eichelberger, J.C., & Rutherford, M.J. (2000). Magma storage and mixing conditions for the 1953-1974 eruptions of Southwest Trident volcano, Katmai National Park, Alaska. *Contributions of Mineralogy and Petrology* **140**, 99-114.

Crank, J. (1975). *The Mathematics of Diffusion, Second Ed.* Oxford University Press, Oxford, England, 414p.

Defant, M. J. & Drummond, M. S. (1990). Subducted lithosphere-derived andesite and dacite rocks in young volcanic arc settings. *Nature* **347**, 662-665.

Demény, A., Vennemann, T. W., Harangi, S., Homonnay, Z. & Forizs, I. (2006). H_2O-δD-Fe^{III} relations of dehydrogenation and dehydration processes in magmatic amphiboles. *Rapid Communication in Mass Spectrometry* **20**, 919-925.

Dobson, P. F., Epstein, S. & Stolper, E. M. (1989). Hydrogen isotope fractionation between coexisting vapor and silicate glasses and melts at low pressure. *Geochimica et Cosmochimica Acta* **53**, 2723-2730.

Dilles, J. H. (1987). Petrology of the Yerington batholith, Nevada; evidence for evolution of porphyry copper ore fluids. *Economic Geology* **82**, 1750-1789.

Eggler, D. H. & Burnham, C. W. (1973). Crystallization and fractionation trends in the system Andesite-H_2O-CO_2-O_2 at pressures to 10 kb. *Geological Society of America Bulletin* **84,** 2517-2532.

Ernst, W. G. & Liu, J. (1998). Experimental phase-equilibrium study of Al- and Ti-contents of calcic amphibole in MORB - A semiquantitative thermobarometer. *American Mineralogist* **83**, 952–969.

Feeley, T. C. & Sharp, Z. D. (1996). Chemical and hydrogen isotope evidence for in situ

dehydrogenation of biotite in silicic magma chambers. *Geology* **24**, 1021-1024.

Fifarek, R. A. & Rye, R. O. (2005). Stable-isotope geochemistry of the Pierina high-sulfidation Au–Ag deposit, Peru: influence of hydrodynamics on SO_2 –H_2S sulfur isotopic exchange in magmatic-steam and steam-heated environments. *Chemical Geology* **213**, 253-279.

Fujimaki, H., Tatsumoto, M. & Aoki, K. (1984). Partition coefficients of Hf, Zr, and REE between phenocrysts and groundmasses. *Journal of Geophysical Research* **89**, 662-672.

Giggenbach, W. F. (1992). Isotopic shifts in waters from geothermal and volcanic systems along convergent plate boundaries and their origin. *Earth and Planetary Science Letters* **113**, 495–510.

Giggenbach, W. F. (1997). The origin and evolution of fluids in magmatic-hydrothermal systems. In: Barnes, H. L. (ed.) *Geochemistry of hydrothermal ore deposits, 3rd ed.* New York, John Wiley and Sons, 737-796.

Ghiorso, M. S. & Evans, B. W. (2008) Thermodynamics of rhombohedral oxide solid solutions and a revision of the fe-ti two-oxide geothermometer and oxygen-barometer. *American Journal of Science* **308**, 957-1039.

Graham, C. M., Harmon, R. S. & Sheppard, S. M. F. (1984). Experimental stable isotope studies - hydrogen isotope exchange between amphibole and water. *American Mineralogist* **69**, 128-138.

Grove, T. L., Elkins-Tanton, L. T., Parman, S. W., Catterjee, N., Muntener, O. & Gaetani, G. A. (2003). Fractional crystallization and mantle-melting controls on calc-alkaline differentiation trends. *Contributions to Mineralogy and Petrology* **145**, 515-533.

Grove, T. L., Baker, M. B., Price, R. C., Parman, S. W., Elkins-Tanton, L. T., Chatterjee, N. & Muntener, O. (2005). Magnesian andesite and dacite lavas from Mt. Shasta,

northern California: products of fractional crystallization of H_2O-rich mantle melts. *Contributions to Mineralogy and Petrology* **148**, 542-565.

Harford, C. L. & Sparks, R. S. J. (2001). Recent remobilisation of shallow-level intrusions on Montserrat revealed by hydrogen isotope composition of amphiboles. *Earth and Planetary Science Letters* **185**, 285-297.

Hauri, E., Wang, J., Dixon, J. E., King, P. L., Mandeville, C. & Newman, S. (2002). SIMS analysis of volatiles in silicate glasses 1. Calibration, matrix effects and comparisons with FTIR. *Chemical Geology* **183**, 99-114.

Hedenquist, J. W. & Lowenstern, J. B. (1994). The role of magmas in the formation of hydrothermal ore deposits. *Nature* **370**, 519-526.

Helz, R. T. (1973). Phase relations of basalts in their melting range at P_{H2O} = 5 kb as a function of oxygen fugacity. *Journal of Petrology* **14**, 249–302.

Hildreth, W. & Moorbath, S. (1988). Crustal contributions to arc magmatism in the Andes of central Chile. *Contributions Mineralogy Petrology* **98**, 455–489.

Ingrin, J., & Blanchard, M. (2000). Hydrogen mobility in a single crystal of kaersutite: *EMPG VIII, J. Conf. Abstr* **5**, 52.

Irving, A. J. & Frey, F. A. (1984). Trace element abundances in megacrysts and their host basalts: Constraints on partition coefficients and megacryst genesis. *Geochimica et Cosmochimica Acta* **48**, 1201-1221.

Kay, S. M. & Mpodozis, C. (2001). Central Andean ore deposits linked to evolving shallow subduction systems and thickening crust. *Geological Society of America Today* **11**, 4-9.

Kent, A. J. R., Stolper, E. M., Francis, D., Woodhead, J., Frei, R. & Eiler, J. (2004). Mantle heterogeneity during the formation of the North Atlantic Igneous Province; constraints from trace element and Sr-Nd-Os-O isotope systematics of Baffin Island picrites. *Geochemistry, Geophysics, Geosystems - G^3* **5**, 26 p.

Kesler, S. E., Issigonis, M. J., Brownlow, A. H., Damon, P. E., Moore, W. J., Northcote, K. E., & Preto, V. A. (1975) Geochemistry of biotites from mineralized and barren intrusive systems. *Economic Geology*, **70**, 559-567.

Larson, P. B. & Taylor, H. P. (1986). $^{18}O/^{16}O$ ratios in ash-flow tuffs and lavas erupted from the central Nevada caldera complex and the central San Juan caldera complex. *Contributions to Mineralogy and Petrology* **92**, 146-156.

Larson, P. B. & Geist, D. J. (1995). On the origin of low-^{18}O magmas; evidence from the Casto Pluton, Idaho. *Geology* **23**, 909-912.

Leake, B. E., Wooley, A. R., Arps, C. E. S., Birch, W. D., Gilbert, M. C., Grice, J. D., Hawthorne, F. C., Kato, A., Kisch, H. J., Krivovichev, V. G., Linthout, K., Laird, J., Mandarino, J. A., Maresch, W. V., Nickel, E. H., Rock, N. M. S., Schumacher, J. C., Smith, D. C., Stephenson, N. C. N., Ungaretti, L., Whittaker, E. J. W. & Youzhi, G. (1997). Nomenclature of amphiboles: report of the subcommittee on amphiboles of the International Mineralogical Association, commission on new minerals and mineral names. *American Mineralogist* **82,** 1019-1037.

LePage, L. D. (2003). ILMAT: an Excel worksheet for ilmenite–magnetite geothermometry and geobarometry. *Computers & Geosciences* **29**, 673–678.

Longo, A. A. (2005). Evolution of Volcanism and Hydrothermal Activity in the Yanacocha Mining District, Northern Perú. *Unpublished Ph.D. Dissertation,* Oregon State University, Corvallis, 469 p.

Longo, A. A., Dilles, J. H., Grunder, A. L. & Duncan, R. (2010). Evolution of calc-alkaline volcanism and associated hydrothermal gold deposits at Yanacocha, Peru. *Economic Geology* **105**, 1191-1241.

Lowenstern, J. B. (1995) Applications of silicate melt inclusions to the study of magmatic volatiles. In: Thompson, J.F.H. (ed.) *Magmas, fluids, and ore deposits.* Mineralogical Association of Canada Short Course **23**, 71-100.

Moore, G. & Carmichael, I. S. E. (1998). The hydrous phase equilibria (to 3 kbar) of an andesite and basaltic andesite from western Mexico: constraints on water content and conditions of phenocryst growth. *Contribution to mineralogy and petrology* **130**, 304-319.

Nagasawa, H. & Schnetzler, C. C. (1971). Partitioning of rare Earth, alkali, and alkaline Earth elements between phenocrysts and acidic igneous magmas. *Geochimica et Cosmochimica Acta* **35**, 953-968.

Oberti, R., Ungaretti, L., Cannillo, E. & Hawthorne, F. C. (1993). The mechanism of Cl incorporation in amphibole. *American Mineralogist* **78**, 746-752.

Pallister, J. S., Hoblitt, R. P. & Reyes, A. G. (1992). A basalt trigger for the 1991 eruptions of Pinatubo volcano? *Nature* **356**, 426-428.

Pokrovski, G. S., Borisova, A. Y. & Harrichoury, J-C. (2008). The effect of sulfur on vapor-liquid fractionation of metals in hydrothermal systems. *Earth and Planetary Science Letters* **266**, 345-362.

Richards, J.P. (2011) High Sr/Y arc magmas and porphyry Cu ± Mo ± Au deposits: just add water. *Economic Geology* **106,** 1075-1081

Ridolfi, F., Renzulli, A. & Puerini, M. (2010). Stability and chemical equilibrium of amphibole in calc-alkaline magmas: an overview, new thermobarometric formulations and application to subduction-related volcanoes. *Contribution to Mineralogy and Petrology* **160**, 45-66.

Roedder, E. (1984) Fluid Inclusions. *Reviews in Mineralogy*, Mineralogical Society of America, Washington **12**, 646.

Rohrlach, B. D., & Loucks, R. R. (2005). Multi-million-year cyclic ramp-up of volatiles in a lower crustal magma reservoir trapped below the Tampakan Cu-Au deposit by Mio-Pliocene crustal compression in the southern Philippines. In: Porter, T. M. (ed.) *Super Porphyry Copper and Gold Deposits* **2,** 369-407.

Rowe, M. C., Kent, A. J. R., & Thornber, C. R. (2008). Using amphibole phenocrysts to track vapor transfer during magma crystallization and transport: An example from Mount St. Helens, Washington. *Journal of Volcanology and Geothermal Research* **178**, 593–607

Rutherford, M. J. & Hill, P. M. (1993). Magma Ascent Rates from Amphibole Breakdown - an Experimental-Study Applied to the 1980-1986 Mount St-Helens Eruptions. *Journal of Geophysical Research-Solid Earth* **98**, 19667-19685.

Rutherford, M. J. & Devine, J. D. (2003). Magmatic conditions and magma ascent as indicated by hornblende phase equilibria and reactions in the 1995-2002 Soufrière Hills magma. *Journal of Petrology* **44**, 1433-1454.

Rutherford, M. J. & Devine, J. D. (2008). Magmatic Conditions and Processes in the Storage Zone of the 2004–2006 Mount St. Helens Dacite, Chapter 31: In: Sherrod, D. R., Scott, W. E., & Stauffer, P. H. (eds.) A Volcano Rekindled: The Renewed Eruption of Mount St. Helens, 2004–2006. *U.S. Geological Survey Professional Paper* 1750, 703-725.

Rutherford, M. J, Sigurdsson, H., Carey, S. & Davis, A. (1985). The May 18, 1980, Eruption of Mount St-Helens. 1. Melt Composition and Experimental Phase-Equilibria. *Journal of Geophysical Research-Solid Earth and Planets* **90**, 2929-2947.

Rutherford, M. J., Devine, J. D. & Barclay, J. (1988). Changing magma conditions and ascent rates during the Soufrière Hills eruption on Montserrat. *Geological Society of America Today* **8**, 1-7.

Sato, H., Yamaguchi, Y. & Makino, K. (1997). Cl incorporation into successively zoned amphiboles from the Ramnes cauldron, Norway. *American Mineralogist* **82**, 316-324.

Sisson, T. W. (1994). Hornblende-melt trace-element partitioning measured by ion microprobe. *Chemical Geology* **117**, 331-344.

Sharp, Z. D., Atudorei, V. & Durakiewics, T. (2001). A rapid method for determination of

hydrogen and oxygen isotope ratios from water and hydrous minerals. *Chemical Geology* **178**, 197-210.

Sobolev, V. S. & Kostyuk, V. P. (1975) Magmatic crystallization based on a study of melt inclusions. *Fluid Inclusion Research* **9**, 182-253 (translated from original publication in Russian).

Stormer, J. C. Jr. (1983). The effects of recalculation on estimates of temperature and oxygen fugacity from analyses of multicomponent iron-titanium oxides. *American Mineralogist* **68**, 586–594.

Sun, S. S. & McDonough, W. F. (1989). Chemical and isotopic systematics of oceanic basalts: implications for mantle composition and processes. *Geological Society of London,* Special Publications **42**, 313-345.

Taylor, B. E. (1991). Degassing of obsidian dome rhyolite, Inyo volcanic chain, California. In: Taylor, H. P., O'Neil, J. R. & Kaplan, I.R. (eds.) *Stable isotope geochemistry: A tribute to Samuel Epstein. The Geological Society*, Special publication **3**, 339-353.

Taylor, B. E., Eichelberger, J. C. & Westrich, H. R. (1983). Hydrogen isotopic evidence for rhyolitic magma degassing during shallow intrusion and eruption. *Nature* **306**, 541-545.

Taylor, H. P., Jr. (1997) Oxygen and hydrogen isotope relationships in hydrothermal mineral deposits. In: Barnes, H. L. (ed.) *Geochemistry of Hydrothermal Ore Deposits,* Third Ed., John Wiley and Sons, New York, 229-302.

Teal, L., & Benavides, A. (2010) History and geologic overview of the Yanacocha mining district, Cajamarca, Peru. *Economic Geology* **105**, 1173-1190.

Wallace, P. J. (2005). Volatiles in subduction zone magmas: concentrations and fluxes based on melt inclusion and volcanic gas data. *Journal of Volcanology and Geothermal Research* **140**, 217-240.

Wones, D. R. (1989). Significance of the assemblage titanite + magnetite + quartz in granitic

rocks. *American Mineralogist* **74**, 744–749.

FIGURES AND TABLES

Fig. 1. Geological map of the Yanacocha volcanic field after Longo (2005) and Longo et al. (2010). Hydrothermal breccias are associated with Au (Cu) ores.

Fig. 2. Stratigraphy of the Yanacocha Volcanics listing the phenocryst mineralogy for each magmatic unit, as well as composition, textural type, and sample number of amphiboles analyzed in this study (after Longo, 2005; Chambefort *et al.,* 2008). Abbrevations: *Amph* amphibole, *Anh* anhydrite, *Ap* apatite; *Bt* biotite; *Cpx* clinopyroxene; *KFs* alkali feldspar; *Mt* magnetite (plus ilmenite); *Pl* plagioclase; *Qtz* quartz; *Ttn* titanite.

Fig. 3. Photomicrogaphs of different amphibole textures in the Yanacocha Volcanics. Scale bars represent 500 μm. (a) Atazaico Andesite, sample DO43, resorbed high-Al amphibole with the rim replaced by Fe-Ti oxides. (b) Colorado Pyroclastics, sample DN7, small partially resorbed and decomposed low-Al amphibole with a rim of plagioclase and Fe-Ti oxide. (c) Azufre Andesite, sample CHQS2, decomposed high-Al amphibole with rim of plagioclase, pyroxene, and Fe-Ti oxide. (d) Lower San Jose Ignimbrite, sample RC6, large high-Al amphibole phenocryst without a reaction texture (not resorbed or decomposed) and with anhydrite and apatite inclusions. Small plagioclase crystals are found in equilibrium at the rim of the crystal. (e) Middle San Jose Ignimbrite, sample VC1, small high-Al amphibole (left) with no reaction rim and a decomposed low-Al amphibole with rim of pyroxene, plagioclase, and Fe-Ti oxides (center). (f) Upper San Jose Ignimbrite, sample DE36, partly decomposed high-Al amphibole with an opacite rim of plagioclase and Fe-Ti oxide. Amphibole is partly decomposed along cleavage planes where it is replaced by Fe-Ti oxides. (g) San Jose dome, sample CB3, high-Al amphibole with inclusions of plagioclase but lacking an opacite rim or resorbtion. (h) Coriwachay Dacite, (Corimayo dike), sample

COR1, low-Al amphibole with abundant inclusions of biotite, anhedral plagioclase and Fe-Ti oxides, and without an opacite rim.

Fig. 4. Back-scattered electron images of Yanacocha amphiboles. (a) Atazaico high-Al amphibole. Note the two characteristic breakdown textures: i) the 100-120 μm-thick decomposition zone of fine-grained plagioclase (Pl), pyroxene (Px), and Fe-Ti oxides (O) on the melt interface; and ii) decomposition to bright < 10 μm-wide whitish Fe-Ti oxide "opacite" (OO) along the {110} cleavages in the grain interior. (b) Azufre high-Al amphibole with faint compositional zones normal to the c-axis (elongation), and breakdown textures similar to a). (c, d) Lower San Jose Ignimbrite, sample RC-6, characterized by rare, up to 8 mm long, unzoned, high-Al amphibole lacking zonation or reaction rims, and containing inclusions (d) of abundant anhydrite (Anh) and apatite (Ap). (e) Middle San Jose Ignimbrite, breakdown of high-Al amphibole, core partly reacted to plagioclase and oxides with a rim of coarse oxides that is overgrown by unzoned low-Al amphibole. (f) Upper San Jose Ignimbrite, high-Al amphibole with apatite, Fe-Ti oxide and plagioclase inclusions and irregular anhedral edges. The amphibole shows opacite on cleavages, as in (a). (g) High-Al amphibole of the Upper San Jose Ignimbrite with faint compositional growth zones truncated at the upper edge of the grain, and a fritted edge. (h) Coriwachay Dacite (Corimayo dike) unzoned large low-Al amphibole with abundant biotite (Bt), plagioclase, and rare Fe-Ti oxide inclusions.

Fig. 5. Compositional variations of amphibole in Yanacocha Volcanics. (a) Molar Si/Al_{tot} versus $(Na+K)_A$ per formula unit (p.f.u.). (b) Molar Si/Al_{tot} versus Mg-number molar $(Mg/(Mg+Fe_{tot})$.

Fig. 6. Chondrite-normalized rare earth element patterns for amphibole and whole-rocks from the representative samples of Yanacocha Volcanics and pre-Yanacocha units. Colored and shaded fields are the calculated compositions of melts in equilibrium (eq) with high-Al and low-Al amphibole (see text). (a) Late Coriwachay Dacite. (b-c) Upper San Jose

Ignimbrite. (d) middle San Jose Ignimbrite. (e) Lower San Jose Ignimbrite. (f) Azufre Andesite. (g) Colorado Pyroclastics. (h) Tual and Chaupiloma lower andesite lahars. Chondrite normalization values from Sun & McDonough (1989).

Fig. 7. Trace element patterns for whole-rock and both high-Al and low-Al amphibole normalized to primitive mantle, for the sample DN77 of the Yanacocha porphyry, which is temporally related to the Colorado Pyroclastics. Note negative anomalies for Nb and Zr in high-Al amphibole. The arrows indicate Pb, Sr, Ti and V negative anomalies for the low-Al amphibole compared to the high-Al amphibole. Primitive mantle composition from Sun & McDonough (1989).

Fig. 8. Variations of volatile content in amphibole of the Yanacocha Volcanics. (a) Al_2O_3 (wt %) versus Cl (wt %), (b) Al_2O_3 (wt %) versus F (wt %). (c) H_2O_{SIMS} (wt %) versus F/Cl_{SIMS} of high-Al amphibole plus 3 low-Al amphiboles. Symbols in (a) the same as in (b).

Fig. 9. Zn and Cu content as function of aluminum and chlorine content of high-Al and low-Al amphibole from the Yanacocha Volcanics. (a) Cl (wt %) versus Zn (ppm). (b) Al_2O_3 (wt %) versus Cu (ppm). Whole-rock Zn and Cu contents are from Longo (2005).

Fig. 10. Hydrogen isotope compositions ($\delta D_{V\text{-}SMOW}$, ‰) of amphiboles from the Yanacocha Volcanics. (a) δD_{SIMS} and δD_{TCEA} of amphiboles as a function of the Ar-Ar age of the igneous rocks. (b) δD_{TCEA} of amphibole from the San Jose Ignimbrite. Ar-Ar ages from Longo (2005) and Longo *et al.* (2010).

Fig. 11. Volatile composition obtained by SIMS of the high-Al amphiboles from the Yanacocha Volcanics. (a) H_2O_{SIMS} (wt %) versus δD_{SIMS} (‰). (b) H_2O_{SIMS} (wt %) versus molar Fe^{3+}/Fe_{tot} (calculated from electron microprobe analyses). Arrows represent the general H_2O wt %, δD and Fe^{3+}/Fe_{tot} trends in amphiboles caused by H_2 and H_2O release (Démeny *et al.*, 2006).

Fig. 12. Pressure-temperature stability of Yanacocha amphibole. (a) Stability of amphibole from the Mt. Hood Andesite after Eggler & Burnham (1973). (b) Stability of amphibole

from the Mt. St. Helens dacite from Rutherford *et al*. (1985) and Rutherford & Hill (1993) and Soufrière Hills andesite from Rutherford & Devine (2003). The dashed arrows show the pressure-temperature path of ascending deep-sourced andesite or basaltic andesite (with some heat loss, so not adiabatic). The grey box represents an upper crustal dacite magma chamber, at ~750-850°C and 140 to 220 MPa, which may be heated by underplated andesite to produce amphibole breakdown or rapid eruption without breakdown (two solid arrows).

Fig. 13. Calculated temperatures and oxygen fugacities from Andersen and Lindsley (1985) with reference buffers: Ni-NiO (NNO), hematite-magnetite (Hem-Mag), and Ilmenite+Clinopyroxene = Sphene+Magnetite+Quartz (Dilles, 1987; Wones, 1989). Boundary between SO_2 and H_2S – dominated gaseous sulfur species is calculated from SUPCRT data at a water pressure of 200 MPa.

Fig. 14(a). Water content versus δD for TCEA analyses, showing high-δD , low-δD , and late Coriwachay dacite low δD amphibole fields and paths of amphibole dehydration from Demény et al. (2006) and low-temperature alteration. (b) Illustrating amphibole (Amph) and biotite (Bt) in early andesite and late dacite together with the calculated isotopic composition of water in the corresponding melts. Left arrow shows degassing evolution of melt via Rayleigh distillation with a melt-water fractionation of -20‰, and right illustrates mixtures of andesite melt with hydrothermally altered wall-rock consisting of 50% quartz (Qz) and 50% alunite (Al) and kaolinite (Kao).

Fig. 15. Simplified schematic evolution of the Yanacocha magma chambers through time. (a) Rise of deep-sourced basaltic andesite magma, erupted only in the Atazaico and Azufre Andesites. (b) Prior to the eruption of the ignimbrites, basaltic andesite magma was injected into (or ponded below) a dacite magma body that contained crystallized low-Al amphibole. A new input of deep-sourced mafic magma, with high-Al (δD = ~ -20 to -45‰), likely triggered the next ignimbrite eruption. (c) Assimilation of older hydrothermally altered

Yanacocha Volcanics with a light isotopic composition ($\delta D = -100‰$) into the shallow dacitic magma chamber.

Appendix: sample coordinates

Sample	Ages (Ma)	Units	Composition	UTM position	
Fraile-2	15.51	Cerro Fraile	rhyolite	777413	9234294
DE18	15.41	Tual and Chaupiloma	andesite	774304	9222499
CR4	13.85	Atazaico Andesite	andesite	759388	9230897
DO43	12.28	Atazaico Andesite	andesite	769087	9220508
DN7	12.49	Colorado pyroclastics *Maqui Maqui Ignimbrite*	andesite	774375	9230231
DN77	12.13	Colorado pyroclastics *Porphyry*	andesite	778589	9231823
SLT02	11.90	Colorado pyroclastics *Porphyry*	andesite	771549	9225504
CHQS2	12.05	Azufre Andesite	andesite	777915	9224717
DO60	12.08	Azufre Andesite	andesite	767427	9224459
RC6	11.51	Lower San Jose Ignimbrite	dacite	784730	9214580
CB44	11.54	Lower San Jose Ignimbrite	dacite	780426	9228656
RC3		Middle San Jose Ignimbrite	andesite	788089	9216963
VC1	11.22	Middle San Jose Ignimbrite	andesite	787394	9221813
DE36	11.25	Upper San Jose Ignimbrite	dacite	780533	9223947
BS3	11.49	Upper San Jose Ignimbrite	dacite	777942	9223338
CB38	11.29	Upper San Jose Ignimbrite	dacite	781550	9220136
CB3	11.23	San Jose Domes	dacite	782055	9227734
DE2	11.36	San Jose Domes	dacite	780271	9226158
COR1	10.78	Coriwachay Dacite (Corimayo dome)	dacite	771540	9224978
YN1A	9.91	Coriwachay (Yanacocha dacite)	dacite	774230	9228305
NG5	8.43	Negritos Ignimbrite	rhyolite	769555	9237291

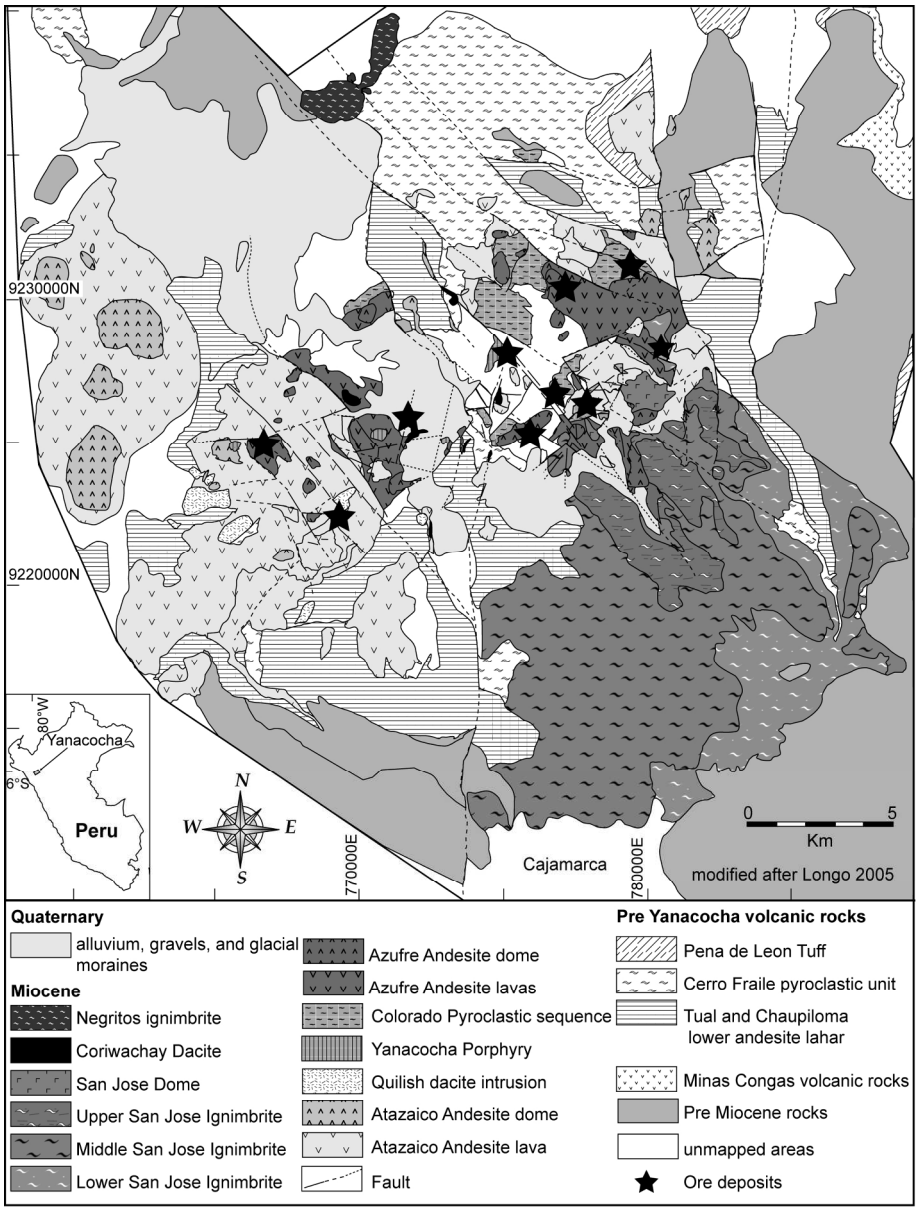

Figure 1
165x218mm (300 x 300 DPI)

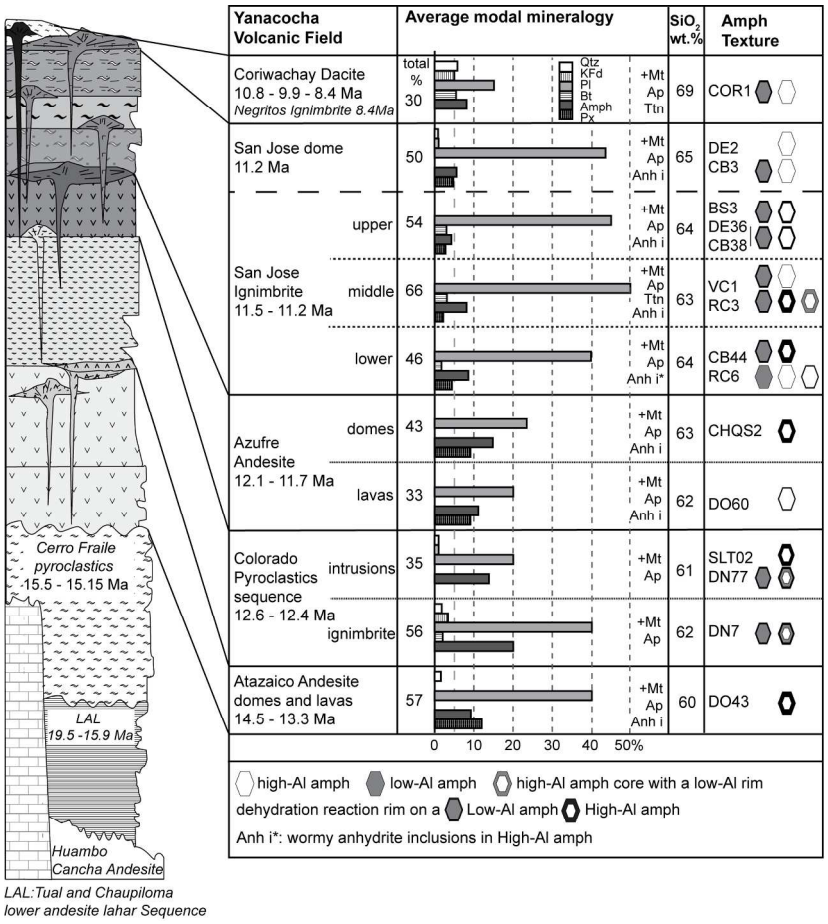

Figure 2
201x184mm (300 x 300 DPI)

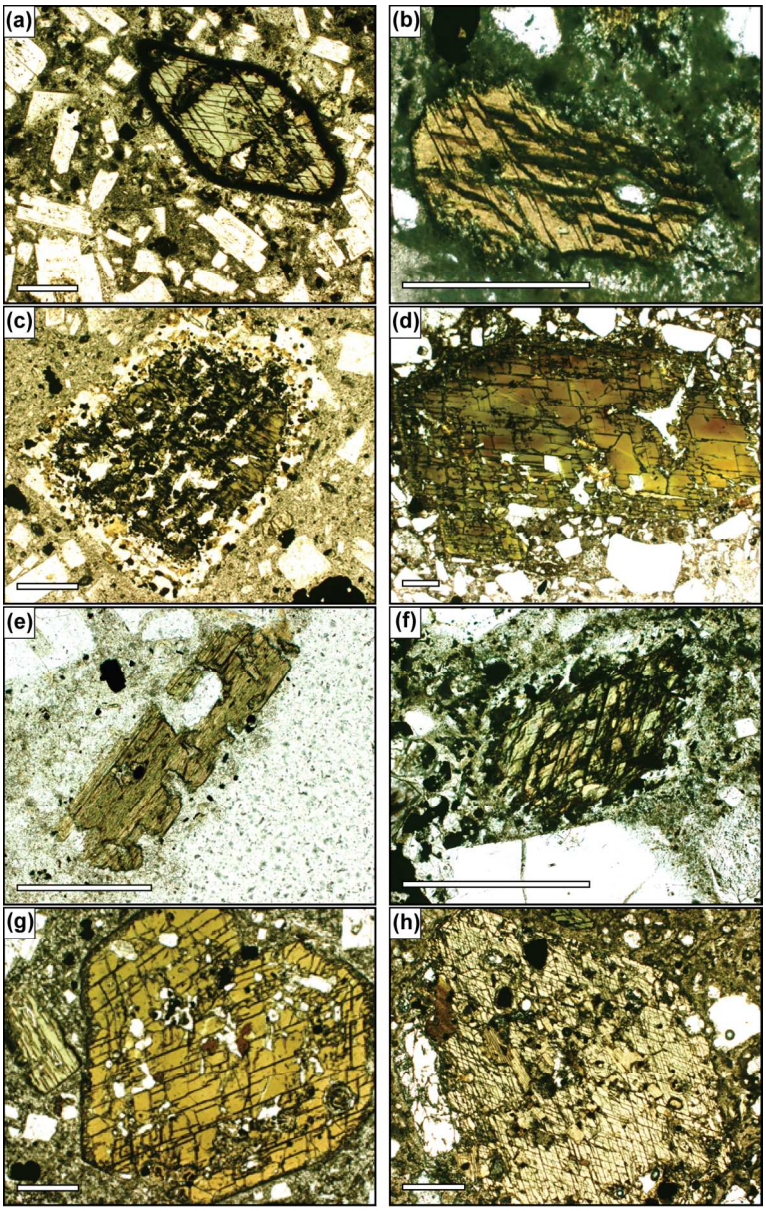

Figure 3
135x214mm (250 x 250 DPI)

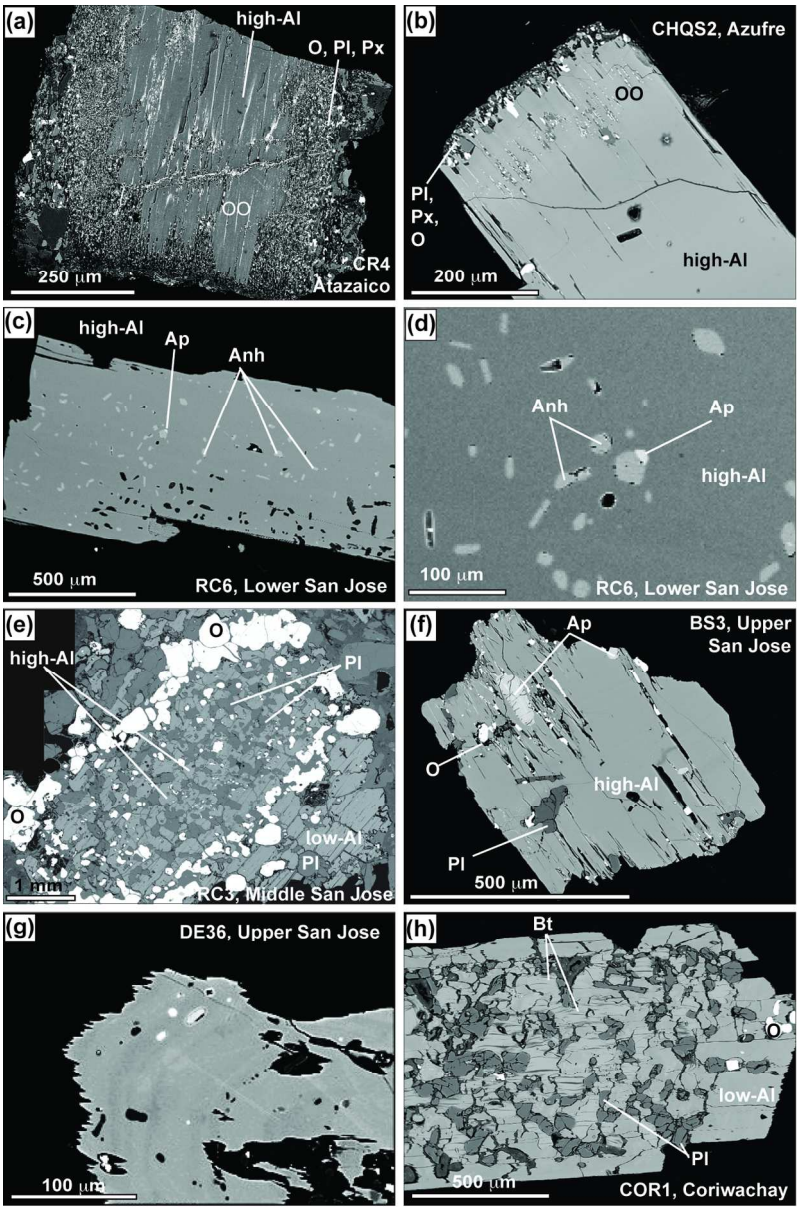

Figure 4
142x215mm (250 x 250 DPI)

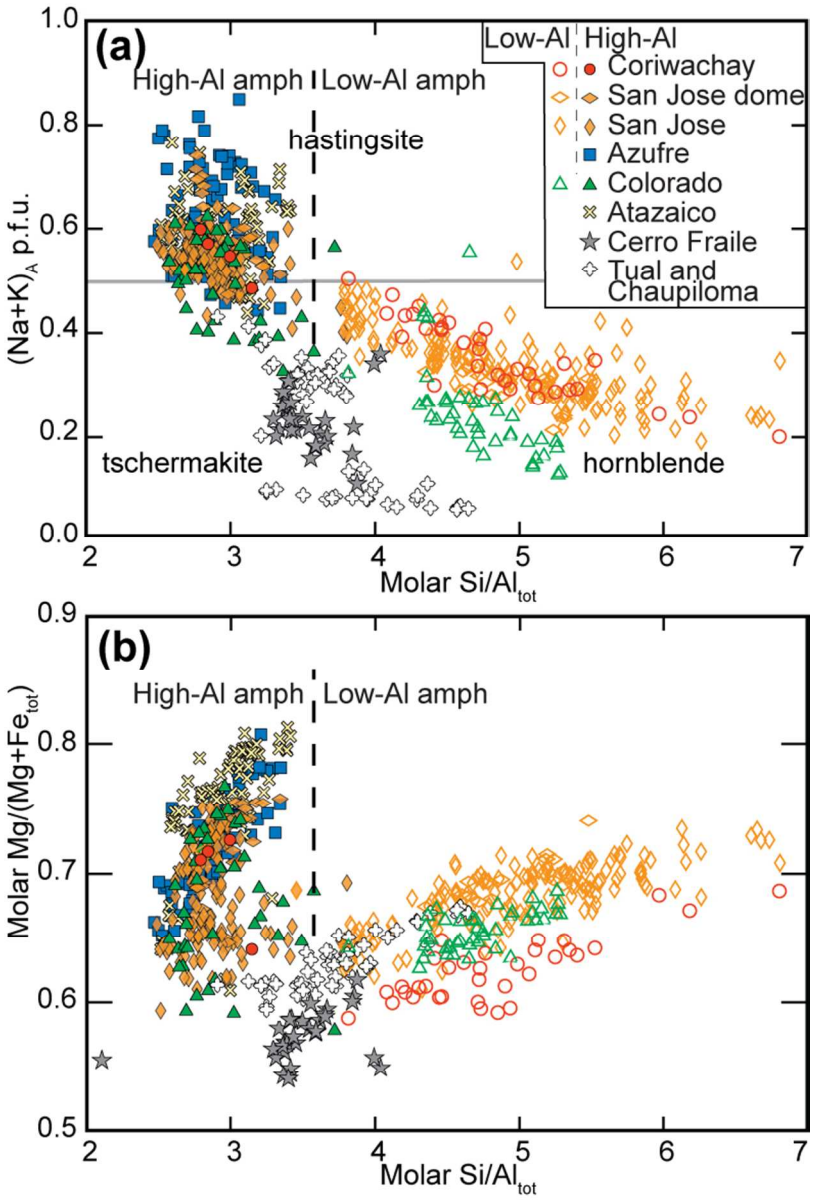

Figure 5
80x119mm (250 x 250 DPI)

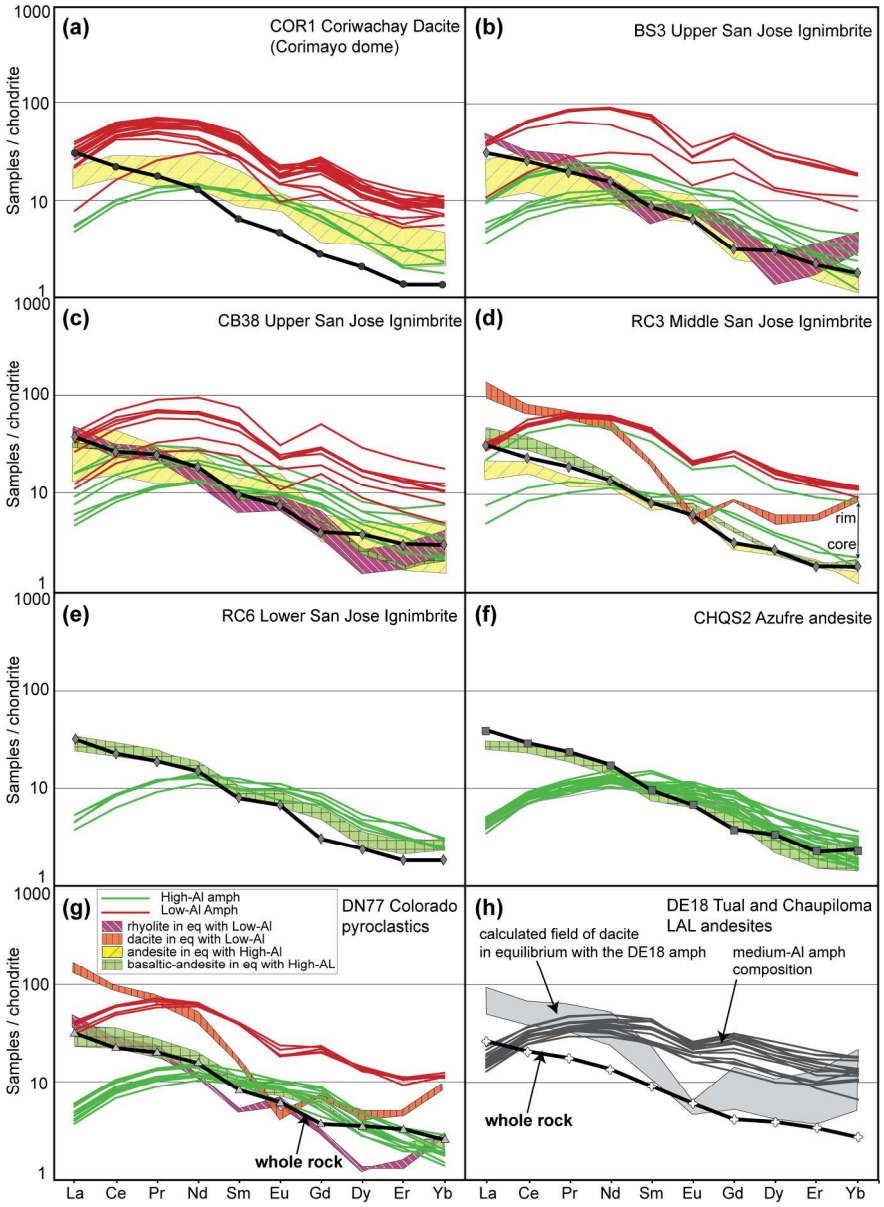

Figure 6
165x226mm (300 x 300 DPI)

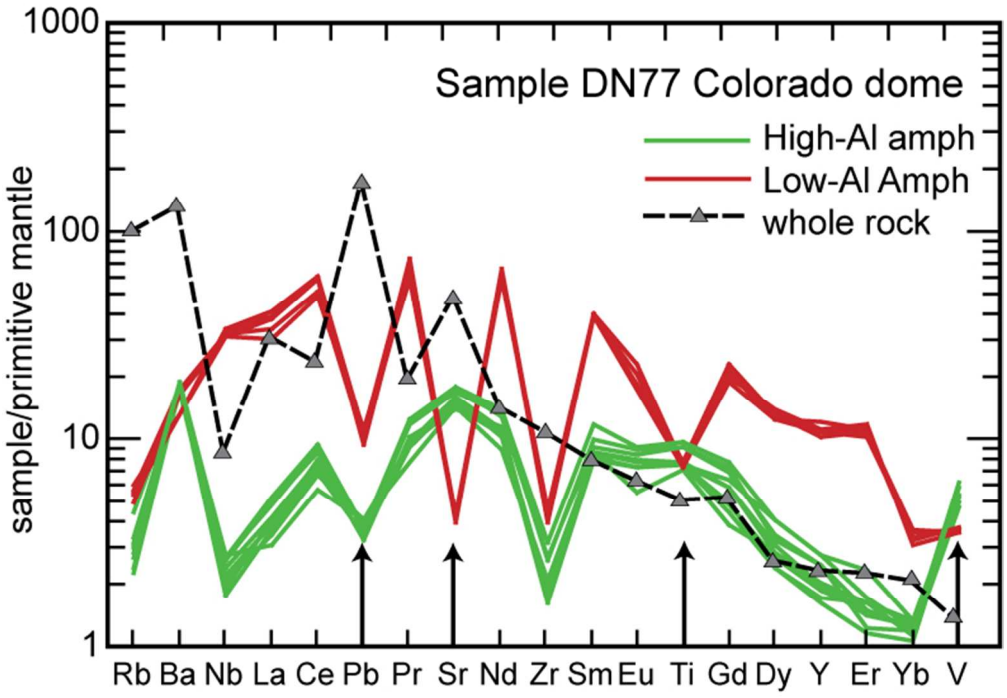

Figure 7
80x55mm (250 x 250 DPI)

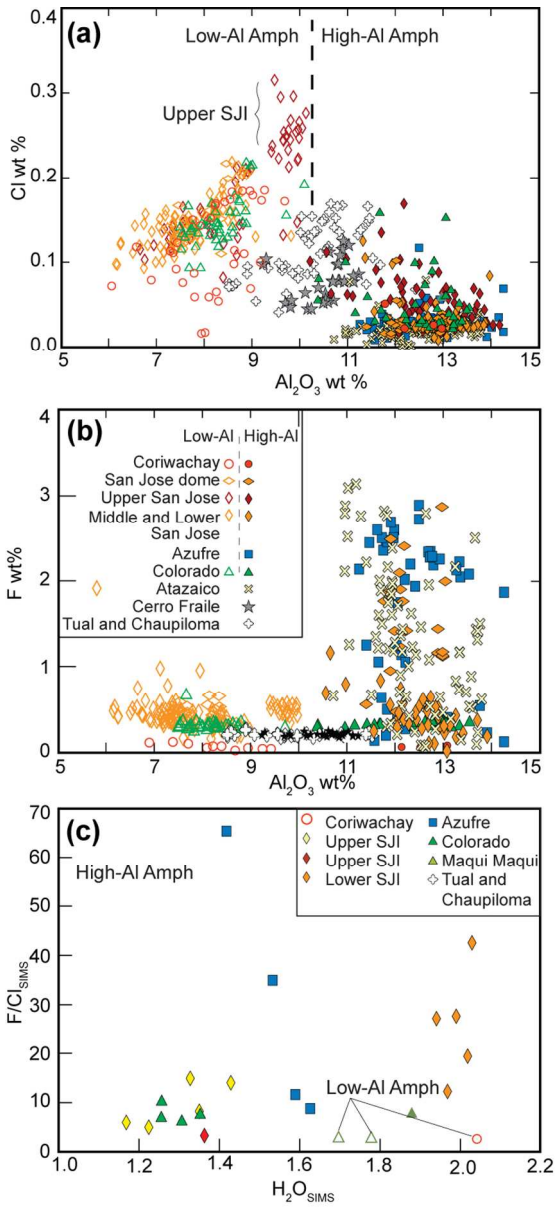

Figure 8
80x175mm (250 x 250 DPI)

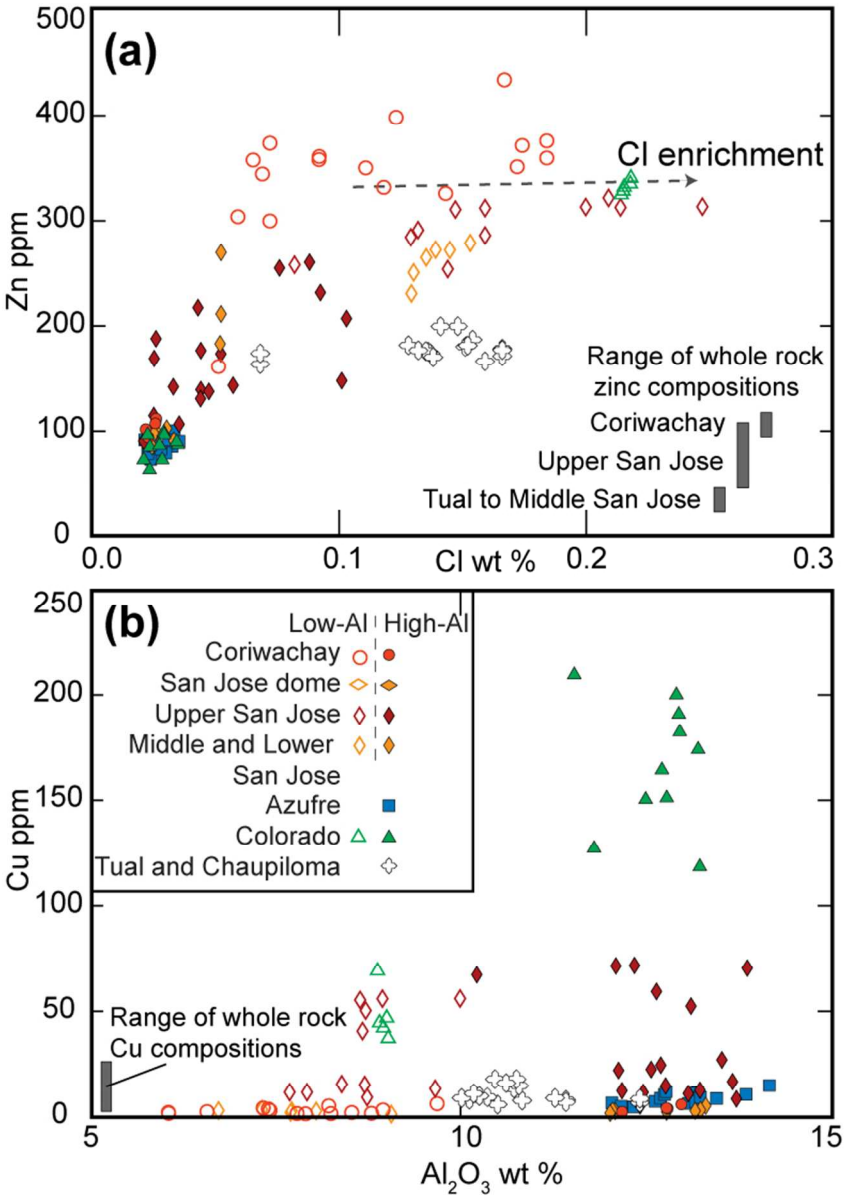

Figure 9
79x114mm (250 x 250 DPI)

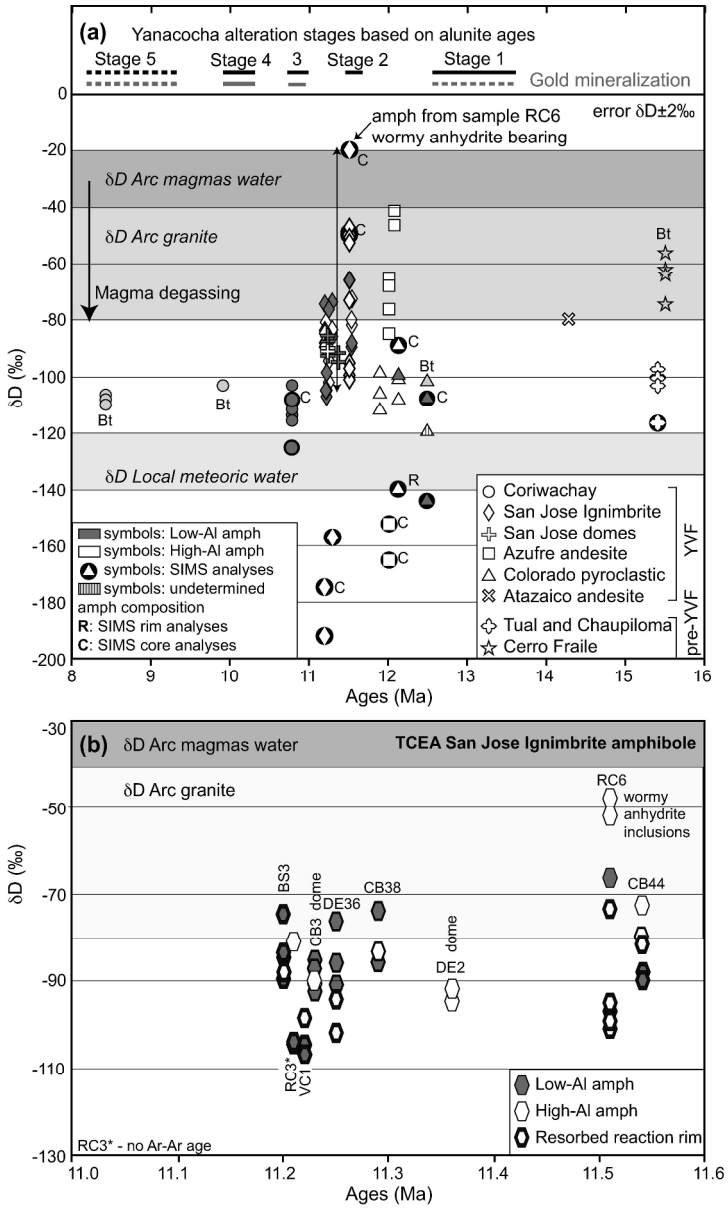

Figure 10
224x373mm (300 x 300 DPI)

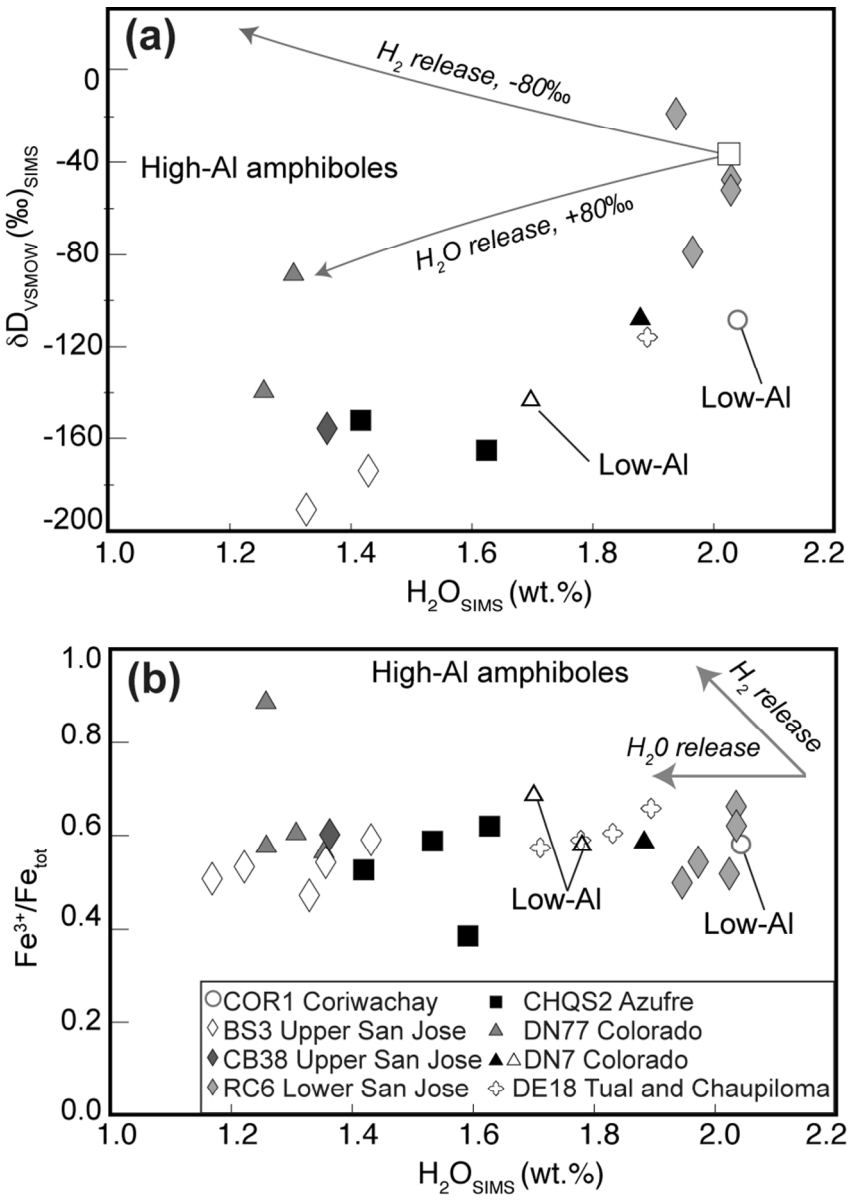

Figure 11

80x113mm (300 x 300 DPI)

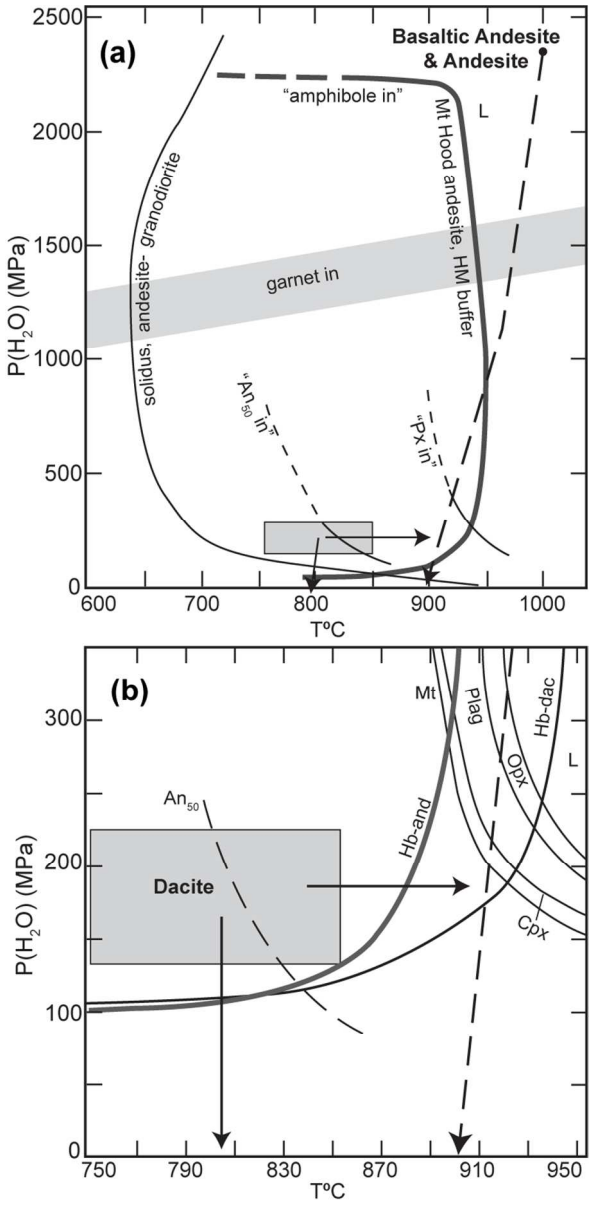

Figure 12
80x165mm (250 x 250 DPI)

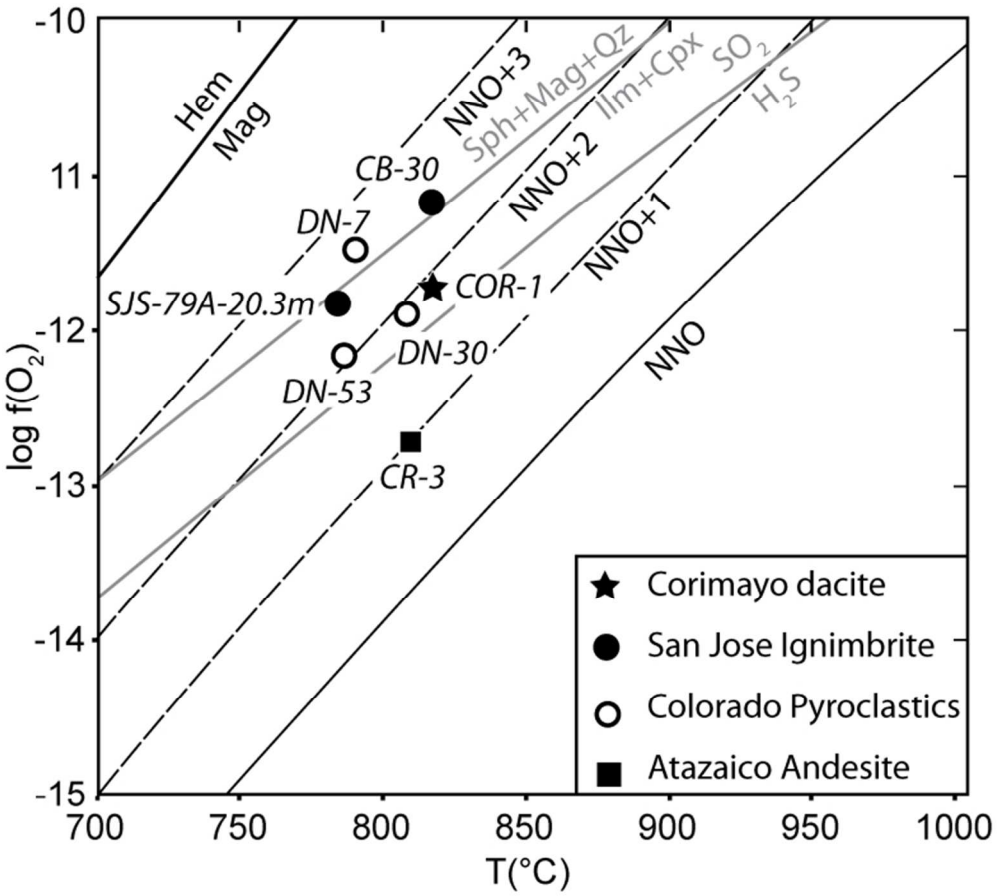

Figure 13
80x71mm (250 x 250 DPI)

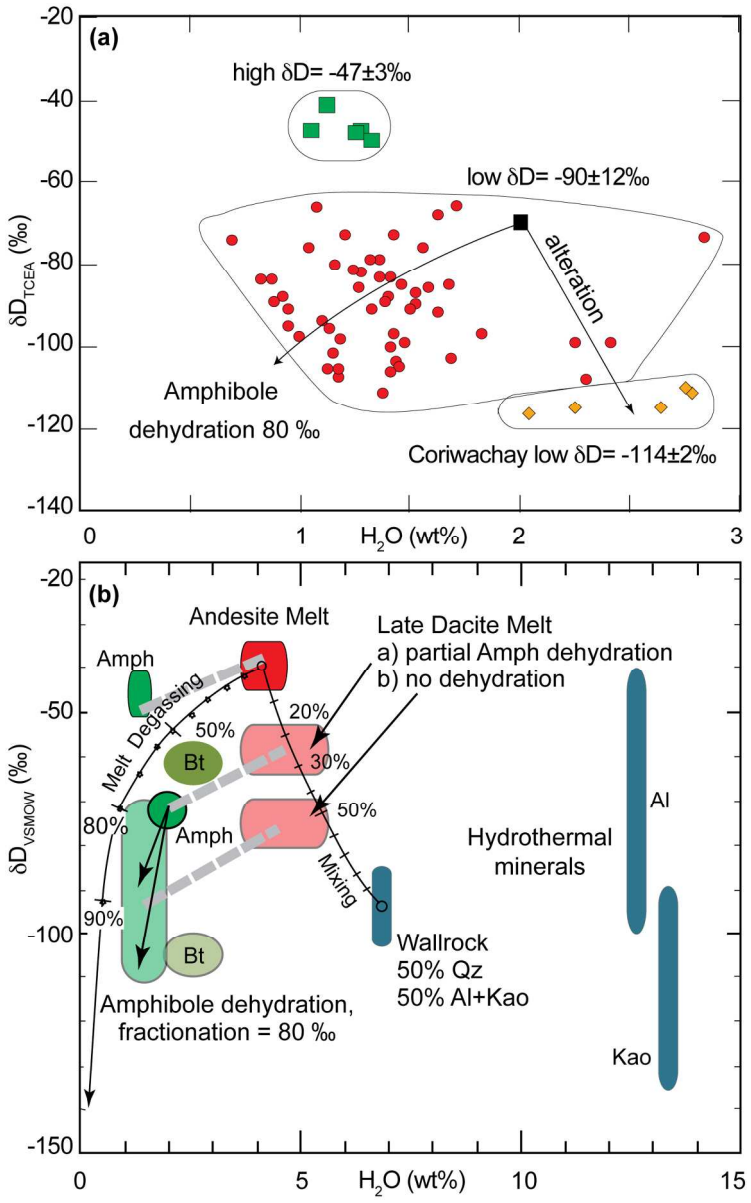

Figure 14
129x209mm (300 x 300 DPI)

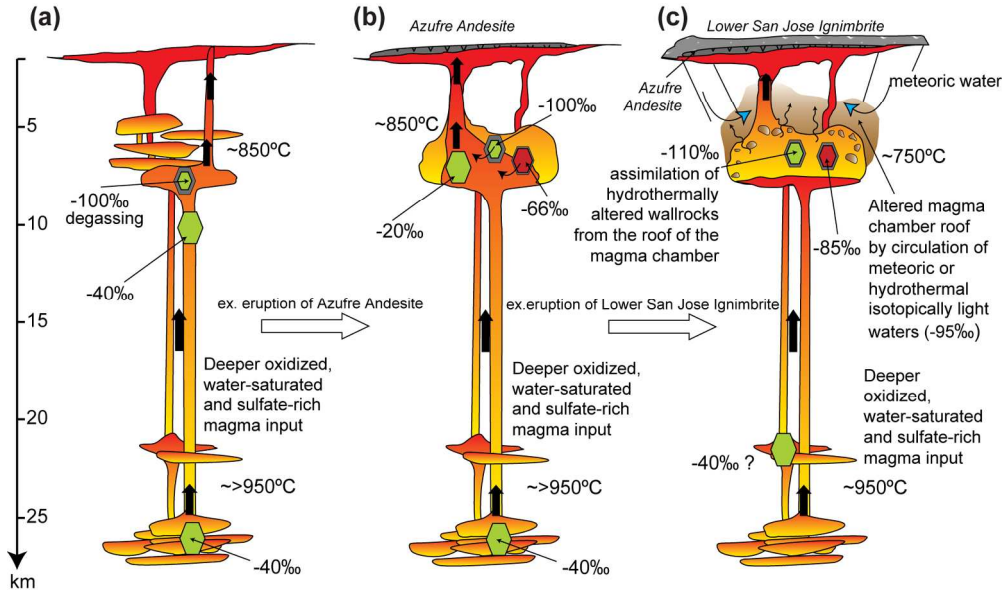

Figure 15
165x97mm (300 x 300 DPI)

Table 1: Representative amphibole analyses by electron microprobe.

UNIT	*Cerro Fraile*	*Tual and Chaupiloma*	*Atazaico Andesite*	*Colorado Pyroclastics*	*Colorado Pyroclastics*	*Azufre Andesite*	*Lower San Jose*	*Lower San Jose*	*Middle San Jose^*
Samples #	Frial2B.4	DE18 6.3	Azu1A 2	DN7 6.1	DN7 4.3	CHQS2A	RC6TS5	RC6 4.2	RC3^ 14
SiO_2	43.93	45.15	43.56	46.99	42.07	40.86	44.96	42.43	46.36
TiO_2	1.05	2.22	1.53	1.31	1.43	2.57	0.00	2.04	1.89
Al_2O_3	10.93	10.12	11.99	7.83	12.41	12.49	9.17	13.61	7.72
FeO	15.33	14.00	7.81	13.37	12.75	9.89	14.86	10.89	11.58
MnO	0.51	0.34	0.12	0.47	0.33	0.18	0.00	0.12	0.36
MgO	12.19	13.51	17.00	15.18	13.41	15.54	14.19	14.43	16.13
CaO	10.61	10.90	11.64	10.99	11.48	12.00	11.15	11.57	11.34
Na_2O	1.60	1.79	2.80	1.33	1.85	2.77	1.72	2.23	1.65
K_2O	0.62	0.61	0.68	0.55	0.75	0.84	0.99	0.81	0.64
Cr_2O_3	0.02	0.00	0.29	0.00	0.14	0.02	0.00	0.00	0.00
F	0.21	0.00	1.27	0.24	0.32	2.80	<DL	<DL	<DL
Cl	0.08	0.13	0.02	0.12	0.05	0.11	0.00	0.03	0.13
Total	97.10	98.79	98.76	98.37	97.03	100.10	97.13	98.16	97.82
Si	6.41	6.46	6.21	6.68	6.15	5.95	6.54	6.08	6.63
Al^{IV}	1.59	1.54	1.78	1.31	1.84	2.04	1.46	1.92	1.30
Al^{VI}	0.29	0.16	0.23	0.00	0.30	0.10	0.11	0.38	0.00
Ti	0.12	0.24	0.16	0.14	0.16	0.28	0.00	0.22	0.20
Cr	0.00	0.00	0.03	0.00	0.01	0.00	0.00	0.00	0.00
Fe^{3+}	1.17	0.95	0.72	1.23	0.94	0.67	1.21	0.78	0.99
Fe^{2+}	0.70	0.72	0.21	0.36	0.61	0.53	0.60	0.52	0.40
Mn	0.06	0.04	0.01	0.06	0.04	0.02	0.00	0.01	0.04
Mg	2.65	2.88	3.61	3.22	2.92	3.37	3.08	3.08	3.44
Ca	1.66	1.67	1.78	1.67	1.80	1.87	1.74	1.78	1.74
Na	0.45	0.50	0.77	0.37	0.52	0.78	0.49	0.62	0.46
K	0.12	0.11	0.12	0.10	0.14	0.15	0.18	0.15	0.12
F	0.10	0.00	0.57	0.11	0.15	1.29	0.00	0.00	0.00
Cl	0.02	0.03	0.01	0.03	0.01	0.03	0.00	0.01	0.03
OH*	1.88	1.97	1.42	1.86	1.83	0.67	2.00	2.00	1.98
Na_B	0.34	0.33	0.22	0.33	0.20	0.12	0.27	0.22	0.26
$(Na+K)_A$	0.23	0.28	0.68	0.14	0.47	0.81	0.40	0.54	0.31
$Mg^{\#}$	0.59	0.63	0.94	0.67	0.82	0.86	0.63	0.70	0.71
Al^{T}	1.88	1.71	2.01	1.31	2.14	2.14	1.57	2.30	1.30

UNIT	*Middle San Jose**	*Upper San Jose*	*Upper San Jose*	*Upper San Jose*	*Upper San Jose*	*San Jose Dome*	*San Jose Dome*	*Coriwachay Dacite*	*Coriwachay Dacite*
Samples #	RC3* 33	CB38 1	CB38 8	DE36 1	DE36 9	CB3 1.1	CB3 3.3	COR1 3.2	COR1 2.1
SiO_2	42.70	42.68	44.89	41.82	44.88	47.87	42.23	47.20	42.90
TiO_2	1.77	2.24	1.86	2.36	1.85	1.75	1.83	1.25	2.16
Al_2O_3	12.09	12.55	9.75	12.68	9.66	7.41	12.02	7.80	12.80
FeO	12.61	13.27	13.98	13.58	13.28	10.18	12.95	13.73	10.44
MnO	0.38	0.18	0.31	0.13	0.40	0.33	0.36	0.43	0.14
MgO	14.08	13.54	14.14	13.04	14.18	16.33	13.25	14.16	14.82
CaO	11.55	11.75	11.11	11.90	11.50	11.22	11.01	11.38	11.87
Na_2O	2.06	2.10	1.78	2.16	1.81	1.73	2.09	1.48	2.21
K_2O	0.67	0.88	1.21	0.73	1.07	0.61	0.78	0.54	0.69
Cr_2O_3	0.09	0.04	0.00	0.01	0.02	0.00	0.00	0.00	0.00
F	0.00	0.27	0.56	0.30	0.44	0.43	0.45	0.00	0.00
Cl	0.05	0.06	0.23	0.03	0.24	0.13	0.10	0.06	0.03
Total	98.06	99.57	99.85	98.77	99.37	98.00	97.10	98.03	98.06
Si	6.15	6.12	6.42	6.07	6.46	6.83	6.19	6.80	6.16
Al^{IV}	1.85	1.87	1.57	1.92	1.53	1.17	1.81	1.20	1.84
Al^{VI}	0.21	0.24	0.07	0.25	0.10	0.08	0.27	0.12	0.32
Ti	0.19	0.24	0.20	0.26	0.20	0.19	0.20	0.14	0.23
Cr	0.01	0.00	0.00	0.01	0.01	0.00	0.00	0.00	0.00
Fe^{3+}	0.98	0.78	0.98	0.70	0.77	0.68	0.93	0.79	0.65
Fe^{2+}	0.54	0.80	0.69	0.94	0.82	0.53	0.65	0.87	0.60
Mn	0.05	0.02	0.03	0.01	0.05	0.04	0.04	0.05	0.02
Mg	3.02	2.89	3.01	2.82	3.04	3.47	2.89	3.04	3.17
Ca	1.78	1.80	1.70	1.85	1.77	1.72	1.73	1.76	1.83
Na	0.57	0.58	0.49	0.61	0.50	0.48	0.59	0.41	0.62
K	0.12	0.16	0.22	0.13	0.19	0.11	0.15	0.10	0.13
F	0.00	0.12	0.25	0.14	0.20	0.19	0.21	0.00	0.00
Cl	0.01	0.01	0.05	0.01	0.06	0.03	0.03	0.01	0.01
OH*	2.00	1.86	1.68	1.85	1.73	1.78	1.76	1.99	2.00
Na_B	0.22	0.19	0.29	0.14	0.22	0.28	0.27	0.24	0.17
$(Na+K)_A$	0.48	0.55	0.42	0.59	0.47	0.31	0.47	0.27	0.57
$Mg^{\#}$	0.67	0.78	0.81	0.75	0.78	0.74	0.65	0.65	0.72
Al^{T}	2.05	2.12	1.64	2.17	1.64	1.25	2.08	1.32	2.17

Data from Longo (2005) and this study. Total iron FeO as Fe^{2+}; <DL (less than detection limit).
Structural formula determined using cation charge summing to 46, and Fe^{2+}/Fe^{3+} estimation assuming 13 cations from Leake et al. (1997).
OH*: water by difference assuming 2 cations in the (-OH) group.
^*Sample RC3 has no Ar-Ar age and could be considered lower San Jose Ignimbrite as well.*

Table 2: Yanacocha amphibole SIMS volatile and hydrogen isotope compositions.

UNITS	Samples	Al_2O_3 wt%[1]	H_2O wt%	CO_2 ppm	F ppm	S ppm	Cl ppm	δD_{SMOW} ‰
Tual	DE18-1	10.78	1.83	1077	2406	47	1151	
And	DE18-2	11.96	1.71	496	2145	76	1156	
Chaupiloma	DE18-3	11.35	1.78	13	2247	99	1596	
	DE18-4	10.57	1.89	305	1514	102	1773	-116
Colorado	DN7-1	9.06	1.70	9	2887	39	998	-143
Pyroclastics	DN7-2	8.69	1.78	21	3445	57	1225	
	DN7-3	10.76	1.88	6	3826	66	502	-107
	DN77-1	12.83	1.26	3	2028	37	198	-139
	DN77-2	14.08	1.35	43	1465	35	200	
	DN77-3	14.22	1.26	4	1715	51	246	
	DN77-4	12.88	1.31	5	1884	72	298	-88
Azufre	CHQS2-1	13.75	1.53	4	5954	34	170	
Andesite	CHQS2-3	14.12	1.63	6	2024	67	233	-165
	CHQS2-4	12.36	1.42	6	9653	44	148	-152
	CHQS2-5	13.48	1.59	5	2342	62	204	
Lower	RC6-1	12.75	2.02	5	4256	53	220	
San Jose	RC6-2	12.66	1.94	5	5507	19	204	-19
Ignimbrite	RC6-3	12.48	1.97	5	4640	57	381	-79
	RC6-4.1	13.02	2.03	6	6312	38	148	-49
	RC6-4.2	13.13	2.03	6	6312	38	148	-51
	RC6-5	12.72	1.99	4	5422	24	197	
Upper	CB38-1	13.26	1.36	8	3313	79	1000	-156
San Jose	BS3-1	13.00	1.35	3	4579	67	565	
Ignimbrite	BS3-2	13.32	1.22	4	2322	49	467	
	BS#-3	13.94	1.17	429	2556	47	418	
	BS3-4	13.06	1.43	4	3019	61	215	-174
	BS3-5	12.95	1.33	6	4815	85	319	-191
Coriwachay	COR-1	8.94	2.04	6	3103	5	1198	-108
Dacite	COR-2	n.d	2.09	9	4696	77	340	-126

[1] Electron microprobe analyses.

Detection limits: < 30 ppm for H_2O, < 3 ppm for CO_2, and < 1 ppm for F, S and Cl, standard deviation (2s) δD ± 5‰ (Hauri et al., 2002).

Table 3: Yanacocha amphibole hydrogen isotope compositions.

Sample	Ages (Ma)	Units	Mineral	Al_2O_3 (wt%) [1]	Al^T [2]	δD_{VSSMOW} (TCEA) [3] No Rim	δD_{VSSMOW} (TCEA) [3] □□□	δD_{VSSMOW} (SIMS) [3]	H_2O_{CALC} [4]
Fraile-2	15.51	Cerro Fraile	Bt			-62			2.60
						-64			3.75
						-74			3.95
						-56			2.75
DE18	15.41	Tual and	Amph	10.04	1.69		-103		1.68
		Chaupiloma		10.87	1.83		-97		1.83
				10.36	1.75		-100		4.29
				11.42	1.94		-99		2.25
				10.57	1.71			-116	1.89
DO43	12.28	Atazaico	Amph	13.47	2.27		-79		1.31
		Andesite		13.58	2.28		-79		1.36
DN7	12.49	Colorado	Amph	10.76	1.72			-107	1.88
		pyroclastics		9.06	1.50			-143	1.70
		Maqui Maqui		n.d.		-119			
		Ignimbrite	Bt			-102			
DN77	12.13	Colorado	Amph	9.01	1.52		-99		2.41
		pyroclastics		13.31	2.23		-100		3.06
		Porphyry		12.96	2.18		-108		2.30
				12.83	2.13			-139	1.26
				12.88	2.05			-88	1.31
SLT02	11.90	Colorado	Amph	n.d.		-98			1.18
		pyroclastics		n.d.		-105			1.12
		Porphyry		n.d.		-106			1.42
				n.d.		-111			1.37
CHQS2	12.05	Azufre	Amph	13.14	2.18		-85		1.46
		Andesite		13.19	2.16		-76		1.56
				12.62	2.08		-68		1.63
				13.54	2.26		-66		1.71
				14.12	2.21			-165	1.76
				12.36	2.32			-152	1.42
DO60	12.08	Azufre	Amph	14.26	2.38	-47			1.05
		Andesite		11.65	1.91	-41			1.13
RC6	11.51	Lower	Amph	11.94	2.03	-47			1.27
		San Jose		11.32	1.93		-99		1.47
		Ignimbrite		13.64	2.28	-50			1.31
				13.38	2.29	-48			1.26
				12.47	2.10	-73			1.42
				12.64	2.11		-97		1.42
				11.37	1.94		-95		1.13
				12.53	2.11		-100		1.42
				7.81	1.33	-66			1.07
				12.48	2.25			-79	1.94
				13.13	2.30			-51	2.03
				12.66	2.27			-19	1.94
				13.02	2.27			-49	2.03
CB44	11.54	Lower	Amph	8.58	1.44		-88		1.40
		San Jose		8.68	1.45		-89		1.38
		Ignimbrite		13.91	2.40		-80		1.16
				13.08	2.20	-73			1.20
				11.56	1.95		-82		1.27
RC3	no age	Middle	Amph	7.92	1.34		-104		1.43
		San Jose		7.72	1.30		-105		1.45
		Ignimbrite		12.09	2.05	-81			1.24
VC1	11.22	Middle	Amph	7.38	1.24		-105		1.17
		San Jose		12.58	2.11		-98		1.00
		Ignimbrite		7.45	1.24		-107		1.17
DE36	11.25	Upper	Amph	12.84	2.17		-94		1.10
		San Jose		12.69	2.17		-102		1.15
		Ignimbrite		7.56	1.26	-86			1.26
				7.55	1.27	-91			1.32
				9.96	1.68	-76			1.03
BS3	11.49	Upper	Amph	12.64	2.15		-84		0.87
		San Jose		13.86	2.33		-88		0.92
		Ignimbrite		8.68	1.47		-84		0.82
				8.72	1.50		-89		0.88
				9.92	1.70		-74		0.69
				13.06	2.15			-174	1.43
				12.95	2.30			-191	1.33

CB38	11.29	Upper San Jose Ignimbrite	Amph	12.13	2.05	-83		1.35
				13.23	2.27	-83		1.40
				7.69	1.31	-86		1.59
				8.13	1.40	-74		2.83
				13.26	2.28		-156	1.36
CB3	11.23	San Jose Domes	Amph	7.41	1.25	-92		1.63
				12.03	2.09	-90		1.52
				12.02	2.08	-91		1.5
				8.27	1.41	-87		1.52
				8.36	1.43	-85		1.68
DE2	11.36	San Jose Domes	Amph	12.21	2.01	-95		0.96
				11.91	2.01	-91		0.95
COR1	10.78	Coriwachay Dacite (Corimayo dome)	Amph	6.06	1.03	-116		2.04
				7.80	1.32	-115		2.25
				7.79	1.33	-110		2.75
				6.89	1.16	-112		2.78
				7.35	1.27	-115		2.64
				8.26	1.43	-116		
				7.94	1.37	-112		
				8.94	1.40		-108	2.04
				n.d.	1.60		-126	2.09
YN1A	9.91	Coriwachay (Yanacocha dacite)	Bt			-103		
NG5	8.43	Negritos Ignimbrite	Bt			-108		2.84
						-106		3.50
						-110		2.99

[1] Electron microprobe analysis.
[2] Al atoms per formula unit based on cationic charge summing to 46.
[3] Hydrogen isotopic composition in per mil (‰) relative to V-SMOW.
[4] Water content of amphibole based on H_2 yield from TCEA analysis.
n.d.: not determined

Table 4: Calculated P-T conditions for Yanacocha low-Al amphiboles

Units	**Samples**	**Al**[1] p.f.u	**Si** p.f.u	**Mole %Ab**[1]	**T(°C)**[2]	**P (MPa)**[2]
Colorado	DN7	1.29-1.51	6.78-6.59	58-50	760-820	220-163
Lower SJI	RC6	1.33-1.56	6.74-6.48	66-53	759-824	221-159
Middle SJI	RC3*	1.25-1.47	6.8-6.58	60-50	769-830	167-105
Upper SJI	CB38	1.36-1.50	6.73-6.59	65-57	772-834	207-107
Coriwachay	COR1	1.03-1.53	7.05-6.60	71-62	699-788	173-240

[1] Range of plagioclase compositions by electron microprobe (Longo, 2005)
[2] Results based on iteration using the Anderson & Smith (1995) geobarometer for amphibole with geothermometer of Blundy & Holland (1990) (Hb-Plag thermometry calibration reaction edenite + albite = richterite + anorthite)
Colorado: Colorado pyroclastic sample from the Maqui Maqui Ignimbrite, *SJI:* San Jose Ignimbrite, *Coriwachay:* Coriwachay late Dacite
RC3* sample has no Ar-Ar age and could be considered lower San Jose Ignimbrite as well.

Table 5. Time scales of breakdown reaction and hydrogen diffusion for amphibole

Amphibole corona time						
Amphibole		Experiment Time (days)	Corona width (μm)	Ascent rate[3] (m/sec)	Time (sec)	Time (days)
High-Al[1]	900	20	41	0.003	1.70E+06	20
High/low-Al[2]	830	23	23	0.003	2.04E+06	23
Hydrogen diffusion time						
Amphibole	T(°C)	D (cm^2/sec)[4]	Length (cm)	% D-H Exchange	Time (sec)	Time (days)
High-Al[4]	800	8.6E-10	0.05	>99	2.9E+06	33
High-Al[4]	800	8.6E-10	0.05	50	1.0E+06	11
High-Al[4]	800	8.6E-10	0.25	50	2.4E+07	280

[1] Based on Rutherford & Hill (1993) 2 to 20 day experiments on amphibole breakdown from 160 to 2 MPa (1.6 to 0.02 kb) at 900°C for Mount St. Helens dacite.
[2] Based on Rutherford and Devine (2003) 2 to 23 day experiments on amphibole breakdown from 160 to 2 MPa (1.6 to 0.04 kb) at 830°C for Soufriere Hills andesite,
[3] Ascent rate is based on time from 5 km depth to surface.
[4] Diffusivity, $\ln(D) = \ln(D_o) - Ea/RT(°K)$
[5] Based on plate-like geometry with <1% pore fluid (Crank, 1975; Cole and Ohmoto, 1986), diffusion along the c-axis from Ingrin and Blanchard (2000) for kaersutite at 0.1 MPa at 600 to 900°C and Graham et al. (1984) for actinolite at 200 MPa pressure at 650-850°C.